MICROCOPY RESOLUTION TEST CHART
NATIONAL BUREAU OF STANDARDS-1963-A

DEPARTMENT OF
ATMOSPHERIC SCIENCES
UNIVERSITY OF WASHINGTON

(12)

SCIENTIFIC REPORT

OFFICE OF NAVAL RESEARCH

BRINE DRAINAGE AND CONVECTION

IN YOUNG SEA ICE

by

Terren Mark Niedrauer

DDC

RECEIVED

AUG 22 1977

B

DISTRIBUTION UNLIMITED

July 1977

⑥ BRINE DRAINAGE AND CONVECTION

IN YOUNG SEA ICE,

by

⑩ Terren Mark Niedrauer
Department of Oceanography
University of Washington
Seattle, Washington 98195

⑪ 1977

⑫ 77 p.

⑬ N00014-76-C-0234   ⑭ Scientific -15

370 280

ABSTRACT

In a series of experiments using a 1.6 mm thick freezing tank, thin sections of salt water ice were grown which exhibit the same drainage features as natural sea ice. The tank design permitted photographs to be taken, while thermocouples mounted in the tank walls recorded the temperature profiles within the ice. Convection was observed in both the skeleton layer and in the brine channels by the flow of dyed brine. Flow in the skeleton layer was cusp-like in appearance, consisting of narrow downflow regions separated by broad upflow regions. Several brine channels were usually present in the ice and convective overturning occurred in these channels. The convection caused temperature fluctuations of $0.05°C$, which calculations show increase the vertical heat flux by 2%. The brine drainage channels, which were usually sloped 30° to 60° to the horizontal, always had isotherms tilted from 0° to 13° in the same direction. The brine channels move both horizontally and vertically through the ice by melting their lower walls and freezing on the upper walls. An analysis based on the heat flux due to brine channel convection shows that convection can drive these wall movements. Our observations suggest that most of the brine movement in the channels is caused by recirculation of water from below the ice. We also observed the formation of brine pockets from brine tubes.

TABLE OF CONTENTS

LIST OF FIGURES AND TABLES

iv

v

LIST OF SYMBOLS

All symbols used in the equations are defined in this list. The units are indicated in parenthesis.

A — horizontal cross sectional area (m^2)

c_p — specific heat of brine ($J\ kg^{-1}{}^{\circ}C^{-1}$)

d — diameter (m)

D — salt diffusivity ($m^2 s^{-1}$)

F — convective heat flux (W)

F_c — convective heat flux per unit length ($W\ m^{-1}$)

F_i — conductive heat flux per unit width ($W\ m^{-1}$)

F_1 — latent heat released per unit width ($W\ m^{-1}$)

F_t — total vertical heat flux per unit width ($W\ m^{-1}$)

g — gravitational constant ($m\ s^{-2}$)

H — vertical distance from the top of the tank (m)

k_i — thermal conductivity of ice ($W\ m^{-1}{}^{\circ}C^{-1}$)

L — latent heat of fusion ($J\ kg^{-1}$)

r — radius (m)

S — salinity (o/oo)

T — temperature (°C)

t — time (s)

U — velocity ($m\ s^{-1}$)

x_i — horizontal ice thickness (m)

z — vertical coordinate (m)

ρ_i — ice density ($kg\ m^{-3}$)

γ — viscosity ($m^2\ s^{-1}$)

ACKNOWLEDGMENTS

1. INTRODUCTION

Sea ice, which covers up to 11% of the world ocean, has at least
three large-scale effects. First, in the Antarctic Ocean, the desalina-
tion of sea ice creates cold, salty water which contributes to the
formation of antarctic bottom water. Second, the high albedo of sea ice
reflects and thereby greatly reduces the amount of solar radiation that
would otherwise be absorbed in the polar oceans. Third, the ice acts as
a thermal insulator between the cold air and the warm ocean during the
polar winter, reducing the effect of the ocean as a moderator of climate
in the polar regions.

In the polar spring, over 50% of the world sea ice is less than one
year old. This young ice comprises approximately 75% of the antarctic sea
ice cover and 25% of the arctic cover (Lewis and Weeks 1971). A striking
feature of sea ice is that it is less salty than the ocean water from
which it forms, and becomes fresher as it ages. This has been known since
the first explorers entered the Arctic regions as cited in Malmgren (1927)
and has received considerable attention during the past twenty years (Cox
1974). Through a series of laboratory experiments and a comparison with
field observations, we have documented some important features in the
natural desalination of young sea ice.

In the polar regions, sea ice initially forms when cold air blows
across open water. As the liquid sea surface cools, a slush of ice
crystals forms. As cooling continues, the slush solidifies into a matrix
of randomly oriented ice crystals interlaced with liquid brine. The ice
has a preferential growth direction which results in the ice being

composed of a platelike collection of long, columnar ice crystals with horizontal c-axes growing downward from the surface layer (Weeks 1976). Figure 1, a photograph of the bottom of laboratory sea ice, illustrates the platelike character of the ice bottom. In the lower 10 to 30 mm of the ice, the skeleton layer, brine separates the ice platelets. Higher in the ice, the ice bridges the platelets and brine is isolated in pockets and tubes. This young sea ice, which typically forms in water of 32 $^o/_{oo}$ salinity in the Arctic Ocean, has salinities as high as 25 $^o/_{oo}$ (Malmgren 1927), though 8-12 $^o/_{oo}$ is more common (Cox and Weeks 1974). After one year, desalination further reduces the average ice salinity to about 4 $^o/_{oo}$

Most features of laboratory ice are similar to field ice. The salinity, for example, has an average value of 14 $^o/_{oo}$ for 90 mm thick laboratory ice, which is in the range of the observed field values for ice of comparable thickness. The laboratory ice also has the same structure except that the slush layer thickness is less than 10 mm and hence the dendritic crystals begin growing almost immediately.

Untersteiner (1967) describes the three possible desalination mechanisms for young sea ice; namely brine pocket migration, expulsion, and gravity drainage. The first mechanism postulates that brine in sea ice exists in small pockets between crystals. Under the influence of the temperature gradient, these pockets freeze on the colder side and melt on the warmer side, thus moving along the temperature gradient toward the ice bottom. As noted by Untersteiner (1967), the diffusion rate of salt limits this process so that the migration rate is far too slow to account for the observed brine drainage.
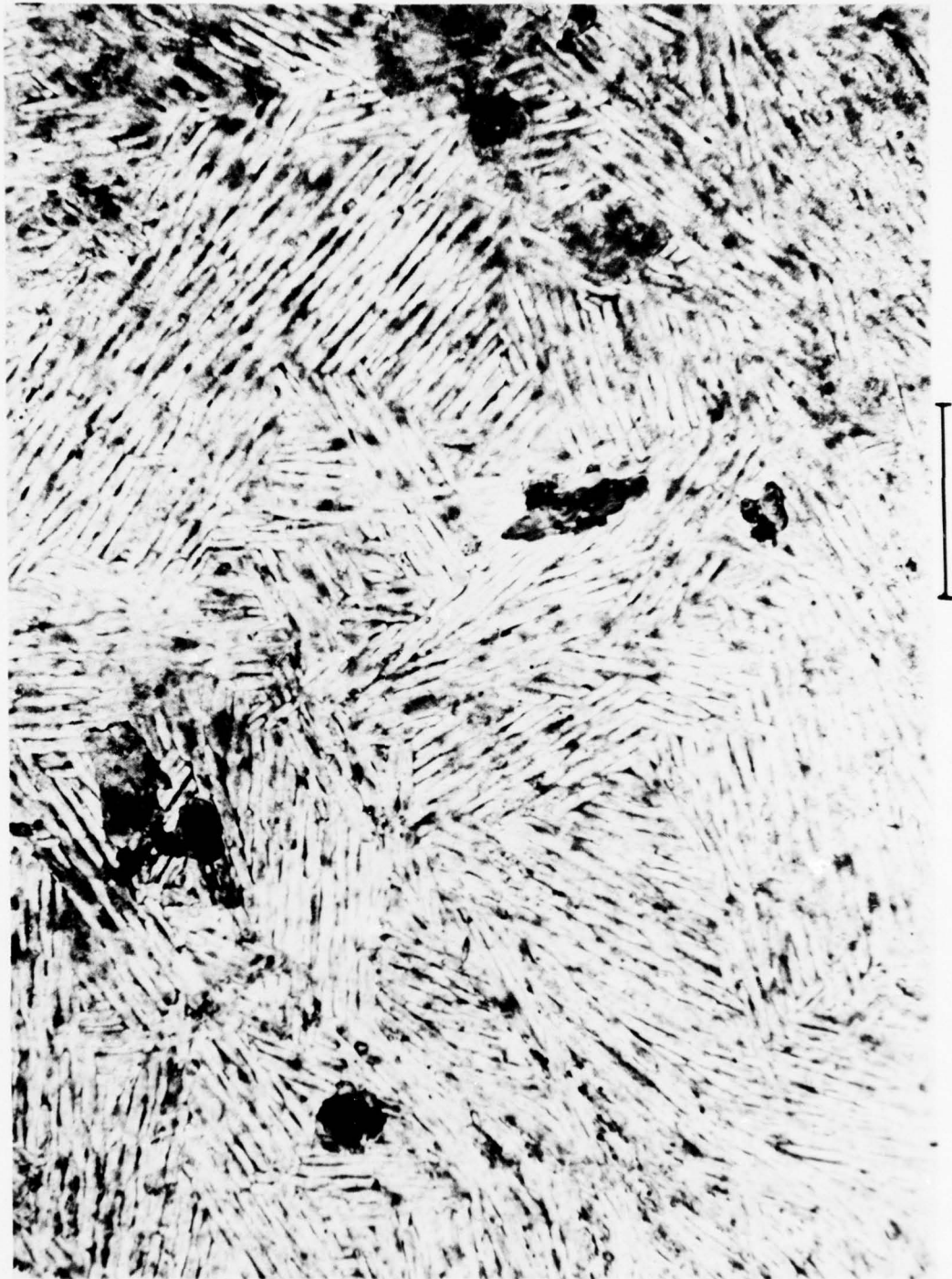
FIGURE 1.   The underside of laboratory sea ice viewed through crossed
polarizing lenses to bring out ice detail. Line on right is 10 mm
in length.

The second mechanism is brine expulsion, which is driven by the cooling of the ice. As the ice gets colder, the brine in the pockets freezes to form more ice so that the remaining brine increases its salinity. Since there is only one temperature at which brine and ice can be in thermodynamic equilibrium, the salinity increase allows the brine to remain liquid at a colder temperature. Because the newly formed ice occupies 10% more volume than the brine, the resultant pressure increase expels the brine through cracks and channels into the seawater. Cox (1974) derived a theoretical model for this process and compared it with his experimental results. He found only minor contributions to desalination except in the first few hours of sea ice growth when the rate of temperature change in the ice was large.

The third mechanism, gravity drainage, occurs when brine drains out of the ice because of hydrostatic pressure differences. Since the sea ice floats above the water level, as the ice grows some of the brine will be lifted above the waterline, and the resultant hydrostatic pressure head will force the brine out of the ice. Because the brine is also denser than the underlying seawater, there can be overturning within the ice. This mechanism also requires the ice to have cracks and channels in it for the brine to move. The laboratory experiments of Cox (1974) and Eide and Martin (1975) suggest that this mechanism is dominant.

Although the preceding two mechanisms point to the importance of brine channels in desalination, no study has yet shown how these channels initially form. Cox's (1974) study used radioactive sodium to follow changes in the salinity profile in the ice, and a thermistor chain to measure temperature, but he was unable to correlate these measurements

with either the ice crystal or brine channel structure. In a related experiment, Eide and Martin (1975) photographed the ice structure, but their photographs are not of sufficient resolution to see how the channels form, and they made no correlation of channel formation with either salinity or temperature profiles. Lake and Lewis (1970) froze a thermistor chain into ice growing in an arctic bay and saw temperature fluctuations which suggested convection in the ice, but again the associated brine channel structure was unknown. The present experiment obtained temperature measurements from a closely spaced array along with a photographic record of the ice structure. This led to direct relations between the thermal history of the ice and the brine channel structure.

The following report first describes in section 2, the experimental equipment and procedure, then examines the thermodynamics of the advancing ice-brine interface in section 3. Section 4 discusses the skeleton layer of the ice and describes the asymmetric cusp phenomena, which is followed in section 5 by a report of brine channel observations and their physics. Finally, section 6 discusses brine tubes and pockets, their metamorphosis, and the implications of this to brine channel formation.

2. THE EXPERIMENT

In our experiment, thin sections of sea ice were grown between two transparent sheets of plastic to permit direct visual observation of the interior of the young ice. The thin cross section made it possible to photograph the entire thickness of the ice without the ice opaqueness hiding important features. The experimental apparatus is similar to that of Eide and Martin (1975) with thermocouples added to measure the temperature inside the ice. The tank is .22 m high and .11 m wide (figure 2). The walls are 12 mm thick "Plexiglas" (polymethyl methacrylate) separated by a 1.6 mm space for the brine. A circulating alcohol bath which cooled a copper plate on top of the tank acted as a heat sink for growing the ice. The top and sides of this tank were further insulated with 50 mm of "Styrofoam" (polyurethane foam).

To minimize heat losses and to permit photography, in the early experiments, we placed 3 layers of thermopane filled with dry nitrogen over the front and back faces of the tank. In later experiments, to improve photographic clarity, we used a vacuum cell instead of the thermopanes as an insulator on the front tank face. The vacuum system had an inner wall of 12 mm plastic against the ice and an outer wall of 6.3 mm thick glass, which is much flatter than the 4 plastic sheets it replaced. The system reached a vacuum of 0.05 torr. Results reported by Dushman (1949) and Brunner and Batzer (1965) indicate that 0.05 torr corresponds to a reduction of the thermal conductivity of air by 95%. The vacuum tank is 0.5 mm thick, which is equivalent to a 10 mm layer of nonconducting dry air at atmospheric pressure. For both kinds of insulation, the
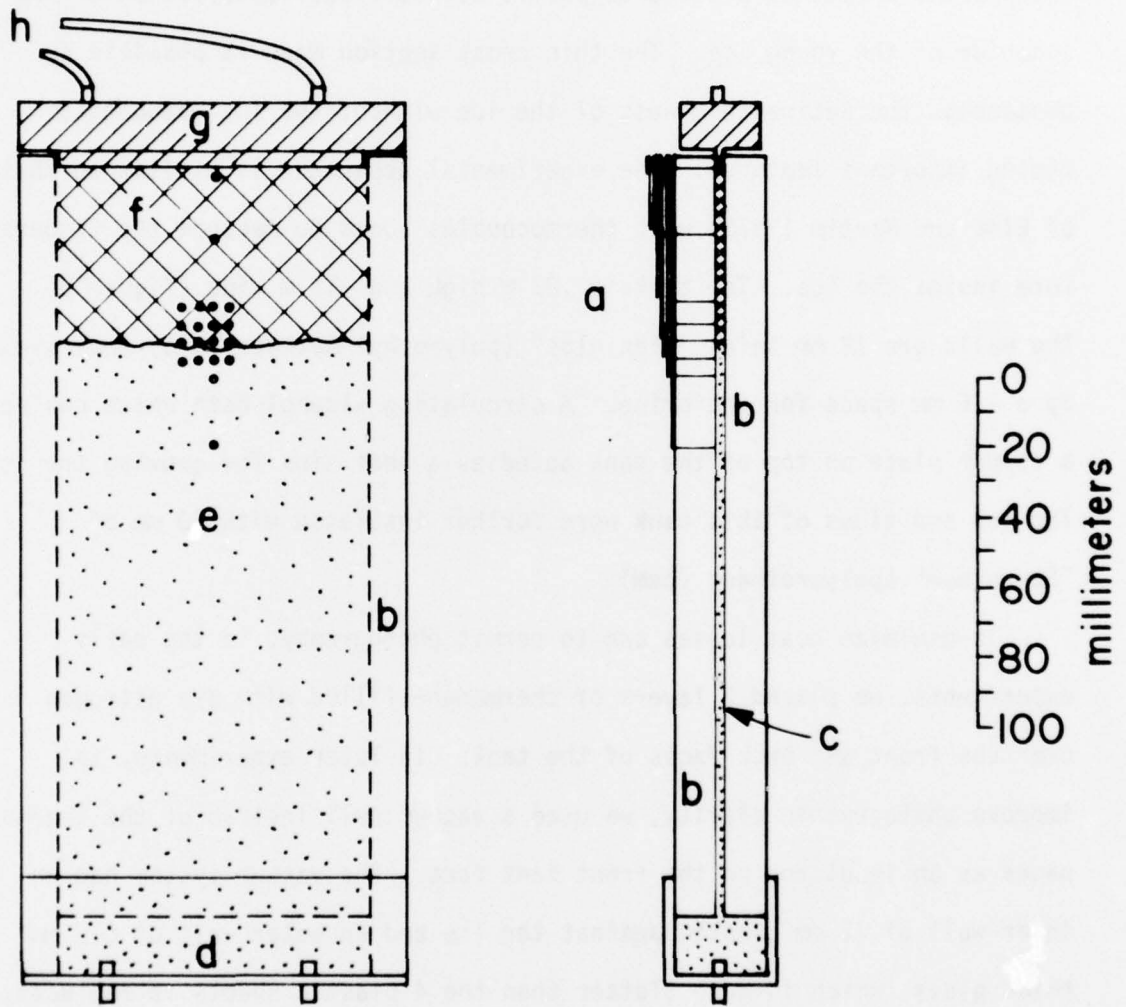
FIGURE 2. Illustration of the experimental tank for growing thin sections of sea ice: (a) thermocouples, (b) Plexiglas, (c) test section, (d) reservoir, (e) 32⁰/₀₀NaCl solution(f) ice, (g) copper cold plate, and (h) tubing to the alcohol cooling bath.

"Styrofoam"-tank unit was placed inside of a box which allowed at least .1 m of free airspace around the unit. The box was insulated with an additional 50 mm of "Styrofoam" (figure 3) which contained a small observation hole for the camera.

The numerous layers of insulation have two roles. First, they reduce the steady flux of heat from the room to the ice; second, they reduce the propagation of thermal transients. The steady sidewall flux determines the depth to which the ice grows, since the ice grows until the heat flux from the sidewalls equals the heat removed by the cold plate (figure 4). An ice depth of 0.1 m was typical for a one day experiment. In natural sea ice, there is no lateral heat flux, except at the edges of the ice pack. By increasing insulation and thus decreasing the sidewall heat fluxes, the laboratory ice more closely resembles natural ice. The sidewall heat flux is also minimized by the plastic walls because the cooling from the top propagates down into the plastic at approximately the same rate at which the ice layer grows. Eide and Martin (1975) arrive at that result by considering the temperature disturbance to travel down a one-dimensional vertical sheet. The equivalent thermal diffusivity for the growing sea ice is approximately the same as the thermal diffusivity for plastic (table 1), so the horizontal temperature gradient between the ice and the walls should be very small. As an example, our temperature measurements showed a difference of 0.1 degree between a probe placed outside of the 12 mm plastic wall and a probe at the same horizontal level in the ice.

The second role of insulation is to dampen the thermal transients. They occur because the laboratory temperature was maintained by a fan which turned on every 15 to 20 minutes to blow air across cooling coils to keep
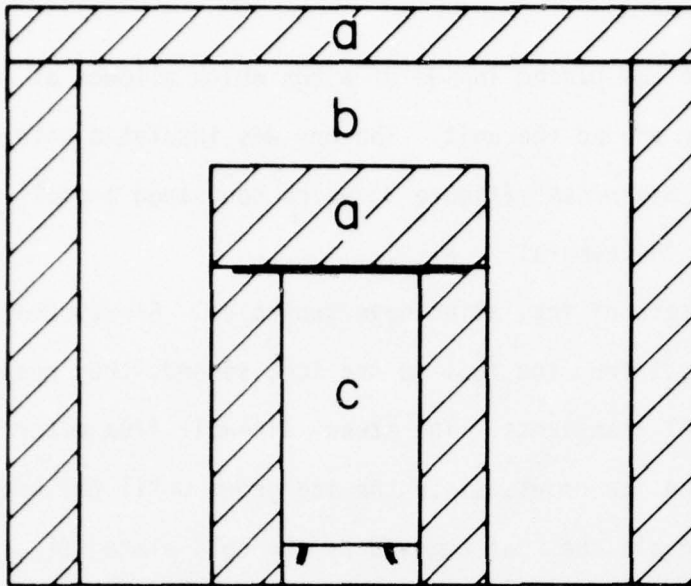
FRONT VIEW

100mm
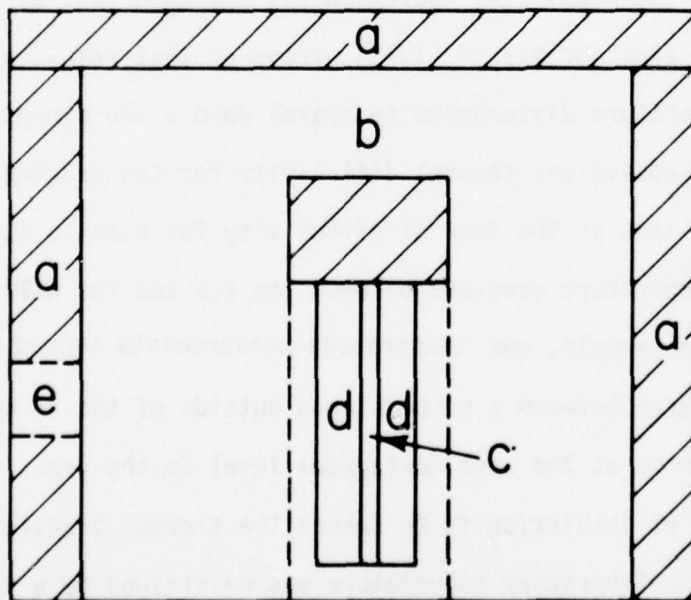
SIDE VIEW

FIGURE 3.   Schematic diagram of insulation surrounding the tank: (a)
Styrofoam, (b) air space, (c) tank, see figure 2, (d) thermopanes,
(e) observation hole.
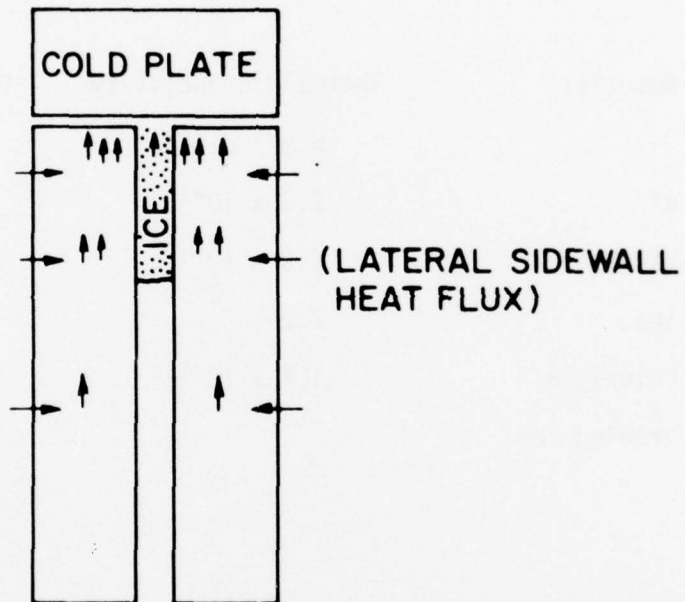
FIGURE 4. A schematic diagram, not to scale, illustrating the balance between the sidewall heat flux and the vertical heat flux through the ice and the plastic.

Table 1. Thermal properties of the materials used in the
construction of the experimental cell (from Eide
and Martin 1975).

Material	Thermal conductivity	Thermal diffusivity
	$W\ m^{-1}\ deg^{-1}$	$m^2\ s^{-1}$
air	2.3×10^{-2}	1.6×10^{-5}
water	5.9×10^{-1}	1.4×10^{-7}
ice	2.2	1.1×10^{-6}
"Plexiglas"	1.7×10^{-1}	1.0×10^{-7}
growing ice		2.2×10^{-7}

the room temperature within ±1°C of the desired temperature. When the fan operates, it mixes the room air within 90 seconds and causes a 1°C to 2°C change in the temperature. Therefore, the final design for the tank insulation was planned to filter out this thermal noise. Measurements made before the outer "Styrofoam" box was put around the tank yielded temperature perturbations with amplitudes up to .25 degrees and a period of 15 to 20 minutes, the same as within the laboratory. When the insulation was put around the tank, temperature fluctuations with this period were no longer detectable.

A desirable effect of having the inner "Plexiglas" walls against the ice was that temperature fluctuations due to brine movement in the ice should be easier to detect. As table 1 shows, the plastic has a lower thermal conductivity than ice, so a temperature change in the brine will propagate more slowly through the walls than through the ice. This gives the temperature probes a longer time to detect a signal since a given temperature change will disperse more slowly than if bounded completely by ice.

Using this tank in a series of experiments, we grew ice from a NaCl-water solution. The reason for using NaCl brine rather than ocean water is that not only is it easier to obtain, but also it models several of the properties of seawater. In ocean water the weight percentages of the salts are 78% for NaCl, 11% for $MgCl_2$, and less than 5% for each of the other individual salts (Neumann and Pierson 1966). The major effect of salts in the formation of ice is freezing-point depression. The freezing point of 35 $^O/_{OO}$ sea water is -1.9°C (Neumann and Pierson 1966), while 35 $^O/_{OO}$ NaCl brine has a freezing point of -2.0°C (Kaufman 1960). The freezing

points are close enough so that the same physical processes should occur
in each case.

One process that occurs differently in ocean water than in NaCl brine
is fractionation. In natural sea ice, fractionation occurs when low tempera-
tures cause one chemical constituent to separate from a solution; for example,
precipitation of Na_2SO_4 occurs at -8.2°C, taking most of the $SO_4^=$ out of
solution. Since $SO_4^=$ is 7.2% of the weight of solids in solution, this can
precipitate 11.4% of the solids when the Na^+ combines with it. At -21.1°C
NaCl precipitates and the Mg salts precipitate below -30°C. Fractionation
did not occur in our experiments because we ran above -21°C. Comparisons
with field data should apply above -8.2°C, and be within 11% for temperatures
less than -8.2°C.

To start an experiment, the tank was filled with a 32 $^o/_{oo}$ NaCl brine
solution. The room temperature was set to -1°C and the entire system was
given a few hours to reach equilibrium. Then the temperature of the
alcohol cooling bath was lowered to -3°C to allow a few millimeters of ice
to form at the top of the cell. When the ice reached a depth of a few milli-
meters, the cold plate temperature was decreased to the final experimental
temperature, typically -17°C. The reason for this procedure is that if the
final cold temperature is set initially, massive supercooling results and
large crystals shoot through the tank. An example of this is illustrated
in figure 5, which is a photograph of an early run. By setting the
temperature just slightly below the freezing point, the water takes longer
to become supercooled, and as time progresses, the probability of the ice
forming increases. Once ice forms, the supercooling problem ceases.

FIGURE 5. Photograph of tank with ice crystals that formed from
supercooled water. The square array has 15 thermocouples
separated by 5 mm. In the background is a horizontal
plastic spacer for the thermocouple wires.

To increase the contrast of the brine drainage features, we would occasionally introduce a small amount of methyl blue dye mixed with seawater into the bottom of the tank. The dye solution, being slightly buoyant, rises to the ice interface to become incorporated into the ice. Any dye remaining in the water was also incorporated into the ice as the interface advanced.

The ice structure was recorded with a movie camera and a time-lapse 35 mm still camera. To minimize the radiant heating of the ice, a 1 watt-second electronic flash unit was used to illuminate the ice. Several 200 watt room lights were kept off during an experimental run, but even when they were turned on, there was no noticeable effect in either the temperature records or the photographs, probably because the insulation around the experiment blocked all of the direct light and most of the indirect light. Opening the door to the laboratory had no noticeable effect since the adjacent room was also refrigerated.

Temperature measurements were made in the ice by means of thermocouples imbedded in the plastic walls. Twenty thermocouples were in the array, 16 of them in a square 4 x 4 grid with a 5 mm spacing and the remainder in a vertical line spaced 20 mm apart (figure 2). The thermocouples protruded slightly (less than .5 mm) from the wall so they would be at the ice temperature and the effect of the plastic on the temperature records would be minimized. A very thin layer of clear plastic insulation was painted over the thermocouples to isolate them electrically from the conductive brine solution. The instruments for reading the thermocouples resolved the temperature to 2.6 mdeg. However, electronic noise was rarely below 10 mdeg, and reached .1 degree occasionally. When we calibrated the array

in a fresh water ice bath, the thermocouples were within 13 mdeg of each other, which is the relative accuracy of any flux measurements. During an experiment, the thermocouples were sampled by a data acquisition system once every one or two minutes. The temperature records were then digitized and stored on a magnetic tape for later processing on a CDC 6400 computer.

Salinity measurements were made in one case by taking the tank apart and cutting the ice into horizontal sections with a knife. The sections were melted and the salinity measured with an optical refractometer. The top section was 10 mm deep with a salinity of 19 $^o/_{oo}$, and the remaining sections were 20 mm deep with salinities of 18, 15, 12, and finally 11 $^o/_{oo}$ in the bottom section, 70-90 mm below the surface. The values from duplicate samples at the same level varied by as much as 2 $^o/_{oo}$.

A study of the photographic and temperature records during an experimental run reveals how the heat is transferred in the tank. When the ice grows, latent heat is released; however, sea ice, particularly in the skeleton layer, is not composed of solid ice, but has a considerable portion of included brine. The majority of the ice forms near the interface, but there is some growth in the interior as it gets colder and the brine volume decreases. Anderson and Weeks (1958) calculate that the skeleton layer of ice has a brine, or liquid volume, V, of at least 15%. Cox (1974) used experimental data to calculate brine volumes in excess of 50% in the lower layer of the ice. Salinity measurements of the lower 20 mm of ice in the present tank indicate a V of 17%. The latent heat released in the lower section of the ice is therefore the amount of heat generated by converting anywhere from .85 to .50 of the brine to ice. The latent heat per unit width released at the interface is computed from

$$F_1 = L\rho_i x_i \frac{\Delta z}{\Delta t}(1 - V) \quad, \tag{1}$$

where L is the latent heat of fusion, ρ_i is the ice density, and x_i is the horizontal ice thickness. The time Δt, it takes the ice front to advance a specified vertical distance Δz, is obtained from photographs.

Assuming the heat is transferred by molecular conduction in sea ice, except for possibly in the bottom 10 mm to 20 mm, then the heat flux per unit width, neglecting the conduction through the brine volume, is calculated from

$$F_i = k_i \frac{dT}{dz} x_i \quad, \tag{2}$$

where T is the temperature, z is the vertical coordinate, k is the thermal conductivity, and the subscript i refers to the solid phase. Measurement of the temperature at two different heights in the ice gives the vertical temperature gradient. Since the ice thickness is known, the heat flux through that section of sea ice can be estimated. If the ice conducted all of the heat generated by the conversion of brine to ice, then the heat flux would be equal to the released latent heat. If it is less, the plastic walls must be conducting some of the released latent heat upward. These calculations were done for several runs, and the results consistently indicate that the ice conducts from 30% to 60% of the heat, depending upon the assumed porosity value (table 2).

The total vertical heat flow in the box, F_t, is the sum of the fluxes through the plastic, F_p, and the ice. This is set equal to the latent heat flux when the horizontal sidewall heating is neglected. For the specific dimensions of the experimental tank, $x_i = 1.6$ mm, $x_p = 25$ mm, and $k_i = 8.7 k_p$

Table 2. Calculations of heat fluxes for 1.6 mm thick ice.

z (mm)	t (sec)	F_1 from eq (1) V = .15 (mW/10 mm)	V = .50 (mW/10 mm)	dT/dz (°C/mm)	F_i from eq (2) (mW/10 mm)	eq (3) F_i/F_1 V = .15	F_i/F_1 V = .50
5	1980	10.35	6.09	.092	2.94	.28	.48
5	2100	9.76	5.74	.11	3.52	.36	.61
5	2400	8.54	5.02	.099	3.17	.37	.63
5	3000	6.83	4.02	.0654	2.09	.31	.52

at -3°C. For the same temperature gradient in the ice and plastic,

$$F_i/F_p = .557 , \qquad F_i/F_t = .36 . \qquad (3)$$

This is in the range of the heat fluxes that were measured in the ice. If the ice porosity were 31%, the predicted and experimental values of F_i/F_t would be the same.

An estimate of the lateral heat flux through the plastic walls is obtained by considering the 0.1°C temperature difference across the 12 mm plastic wall. If we consider a 10 mm by 10 mm section of wall, then the lateral heat flow into the ice will be .21 mW (from equation 2 with the values for plastic). If we compare this value to the latent heat released when the ice interface advances a corresponding distance of 10 mm, we see it is only 5% of the vertical flux at that level. The equilibrium ice thickness can be estimated by equating the length of sidewall heating to the conductive temperature flux that exists when the cold plate is -15°C, the ice bottom is -2.5°C, and assuming the sea ice is solid ice. The thickness is about 100 mm, which agrees well with our observations.

3. THE ICE INTERFACE

Observations of the movement of the ice-brine interface yield an understanding of the thermodynamics of the experiment and provide a further check on the validity of comparisons between laboratory and field ice. For 6 experimental runs, figure 6 gives the position of the ice-brine interface as a function of time. The uncertainties in the measurements are ±2 mm for distance and ±10 minutes for time. The zero on the time axis corresponds to that time when the ice interface is 30 mm from the cold plate, which is the first depth that we could accurately measure. For the run where the 30 mm observation was not available, labeled "x" on the figure, the distance where the earliest observation was made (40 mm) was positioned on the time axis to allow the best fit to the other runs at that position.

Carslaw and Jaeger (1959, section 11.2) describe a simple ice growth model which applies to my experimental tank. They consider a pure liquid at its freezing point in contact with a wall that is at a constant temperature below the freezing point of the liquid. The temperature gradient in the freezing material is assumed linear and the distance, H, of the solid-liquid interface from the cold wall is given by

$$H = (2k_i t\Delta T)^{1/2} (L\rho_i)^{-1/2} , \tag{4}$$

where ΔT is the temperature difference between the wall and the liquid and t is the time from which the liquid starts freezing. Substitution of typical experimental values for ΔT of 15°C and 20°C into the above equations yields the two continuous curves on figure 6.
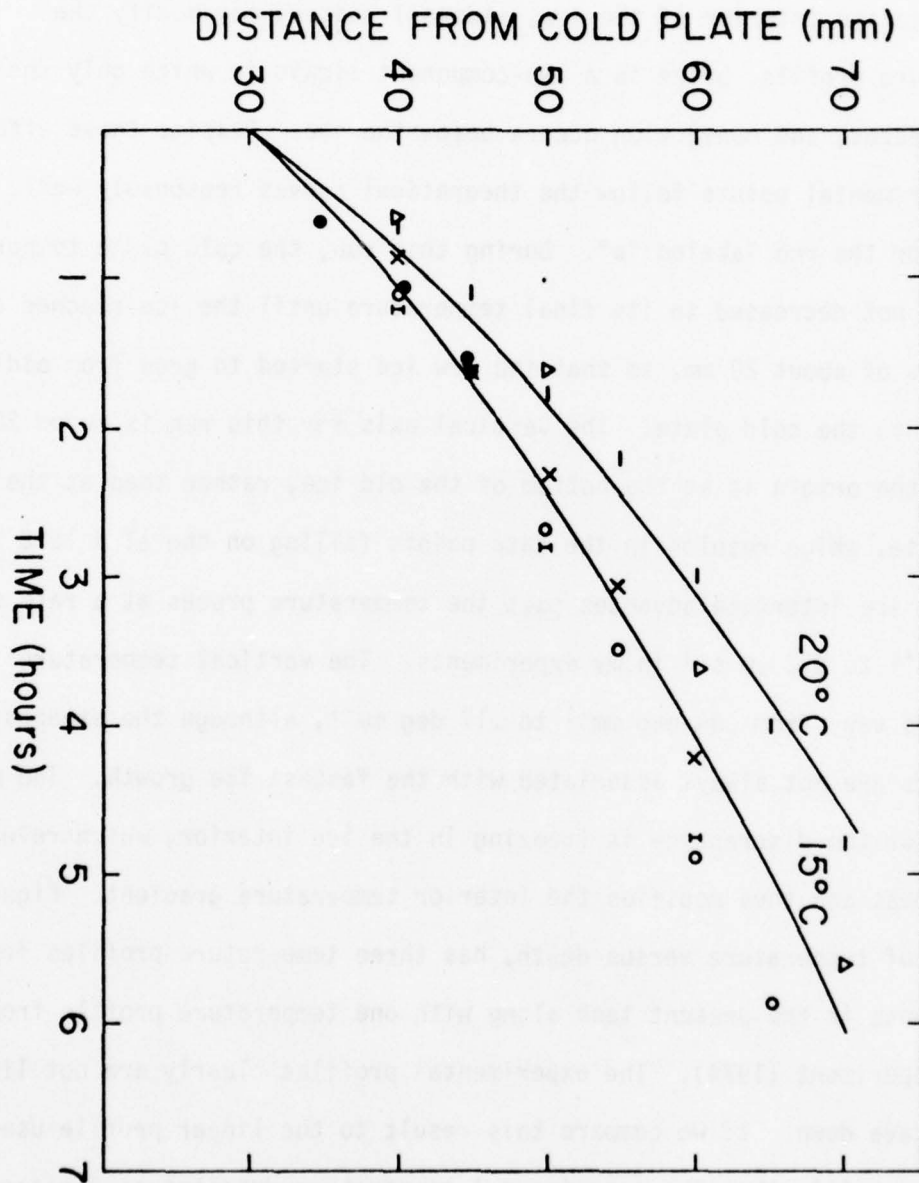
FIGURE 6. Graph of the position of the ice-brine interface relative to the top of the ice as a function of time. Values for ΔT for various runs are: -, 20; ●, 16; Δ, 15; x, 15; I, 14; and o, 12. The solid lines are the theoretical solutions for ΔT = 15 and 20. See text for additional discussion.

Variations of the experimental data from the theoretical curves arise because the cold plate temperature is not set at a specific temperature at a given time, the ice does not freeze solid, there may be some convection in the interior of the ice, sidewall heating may modify the temperature profile, brine is a two-component liquid in which only the water freezes, and convection occurs below the ice. Despite these effects, the experimental points follow the theoretical curves reasonably well, except for the run labeled "●". During this run, the cold plate temperature was not decreased to its final temperature until the ice reached a thickness of about 20 mm, so that the new ice started to grow from old ice, rather than the cold plate. The vertical axis for this run is moved 20 mm so that the origin is at the bottom of the old ice, rather than at the cold plate, which results in the data points falling on the $\Delta T = 15°C$ line.

The ice interface advances past the temperature probes at a rate of 1.1 μm s^{-1} to 5.2 μm s^{-1} in my experiments. The vertical temperature gradients vary from .04 deg mm^{-1} to .17 deg mm^{-1}, although the steepest gradients are not always associated with the fastest ice growth. The major reason for the discrepancy is freezing in the ice interior, which releases latent heat and thus modifies the interior temperature gradient. Figure 7, a graph of temperature versus depth, has three temperature profiles from experiments in the present tank along with one temperature profile from Cox's experiment (1974). The experimental profiles clearly are not linear, but concave down. If we compare this result to the linear profile used in equation (1), then the experimental temperature gradient at the ice bottom is less than expected. One reason for the concave profile is the sidewall heating. From section 2, as the ice gets thicker, the sidewall
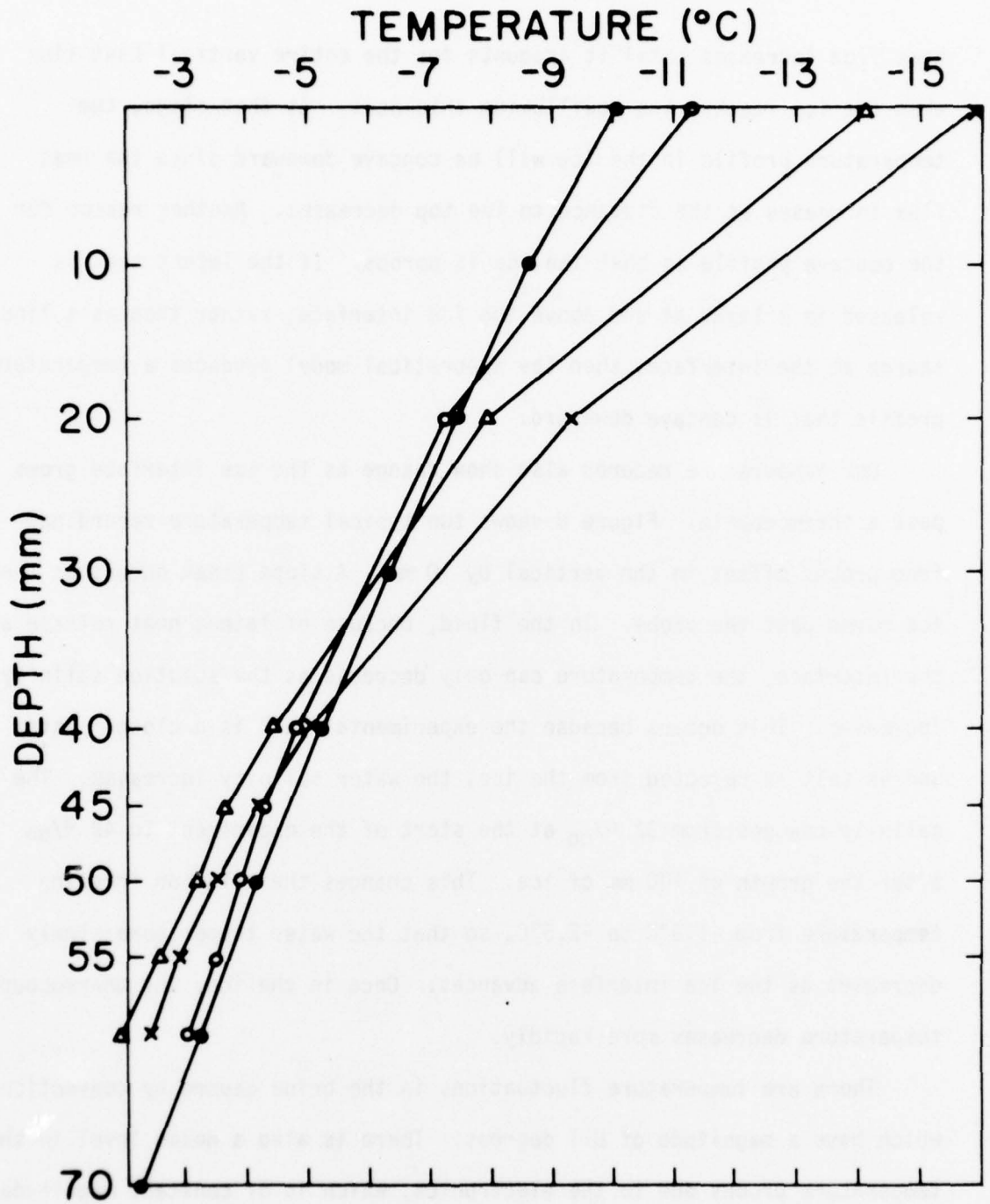
FIGURE 7. Temperature profiles for 3 experimental runs with cold plate
temperatures of -16°C, x; -14°C, Δ; -11°C, o; and a -10°C
run from Cox (1974), ●.

heat flux increases until it accounts for the entire vertical heat flux when the ice reaches its equilibrium thickness. At that stage, the temperature profile in the ice will be concave downward since the heat flux increases as the distance to the top decreases. Another reason for the concave profile is that the ice is porous. If the latent heat is released in a layer at and above the ice interface, rather than as a line source at the interface, then the theoretical model produces a temperature profile that is concave downward.

Our temperature records also show change as the ice interface grows past a thermocouple. Figure 8 shows two typical temperature recordings from probes offset in the vertical by 10 mm. A slope break occurs as the ice moves past the probe. In the fluid, because of latent heat release at the interface, the temperature can only decrease as the solution salinity increases. This occurs because the experimental tank is a closed system and as salt is rejected from the ice, the water salinity increases. The salinity changes from 32 $^o/_{oo}$ at the start of the experiment to 42 $^o/_{oo}$ after the growth of 100 mm of ice. This changes the solution freezing temperature from -1.9°C to -2.5°C, so that the water temperature slowly decreases as the ice interface advances. Once in the ice, the thermocouple temperature decreases more rapidly.

There are temperature fluctuations in the brine caused by convection which have a magnitude of 0.1 degrees. There is also a noise level in the temperature probes due to the electronics, which is of constant magnitude for all probes in a specific experimental run, but varies in magnitude from .01 to .1 degrees depending upon the particular run. The noise level is not affected by the passage of the ice interface, but the convective noise level is decreased (figure 8).
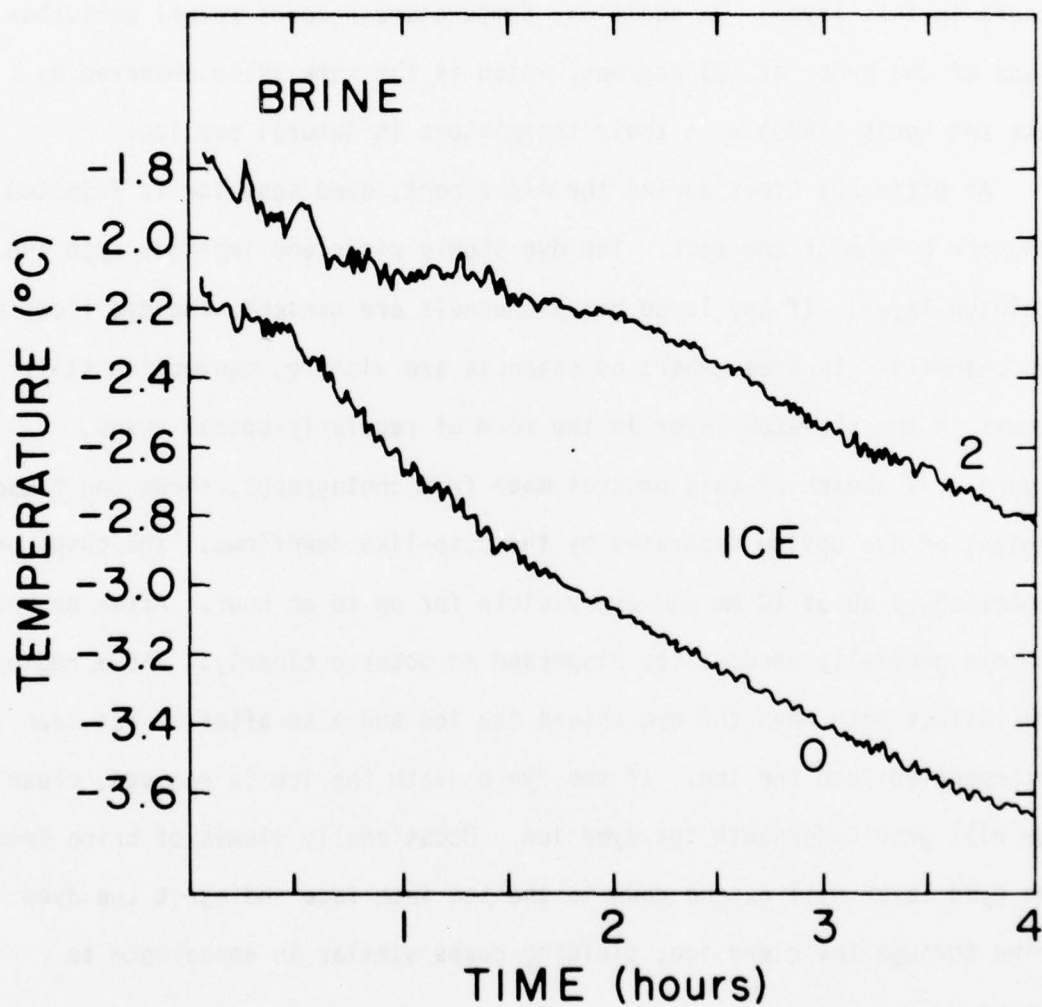
FIGURE 8. A typical temperature record from a thermocouple which shows the slope break when the ice interface passes. The noise level is .02 deg, and the convective perturbations of 0.2 deg are visible on probe 2 before the interface passes. Probes separated vertically by 10 mm.

4. THE SKELETON LAYER

Immediately above the interface is the skeleton layer, a highly porous layer comprising the bottom 10 to 30 mm of the ice. When dye was injected underneath the ice, the photographs reveal that convection occurs in this layer. In addition, temperature records reveal perturbations of the order of .05 degrees, which is the same value observed by Lake and Lewis (1970) with their thermistors in natural sea ice.

At different times during the experiment, dyed seawater is injected into the bottom of the tank. The dye slowly rises and impinges upon the skeleton layer. If any large brine channels are present, the dye flows up the channels. In areas where no channels are visible, convection still occurs in the skeleton layer in the form of regularly-spaced cusps. Figure 9, a sketch of this process made from photographs, shows the broad regions of dye upflow separated by the cusp-like downflows. The cusps are separated by about 10 mm and are visible for up to an hour. After an hour, the dye generally becomes too dispersed to observe clearly. These regions are visible both when the dye enters the ice and also after it has been incorporated into the ice. If the dye beneath the ice is removed, clear ice will grow underneath the dyed ice. Occasionally plumes of brine from the dyed layer will extend down to the ice interface and eject the dyed brine through the clear ice, yielding cusps similar in appearance to figure 9.

The cusps also cause temperature perturbations. In the run shown in figure 10, derived from time-lapse photographs, a cusp to the right of probe 18 moves to the left during a 10 minute interval. The cusp leaves
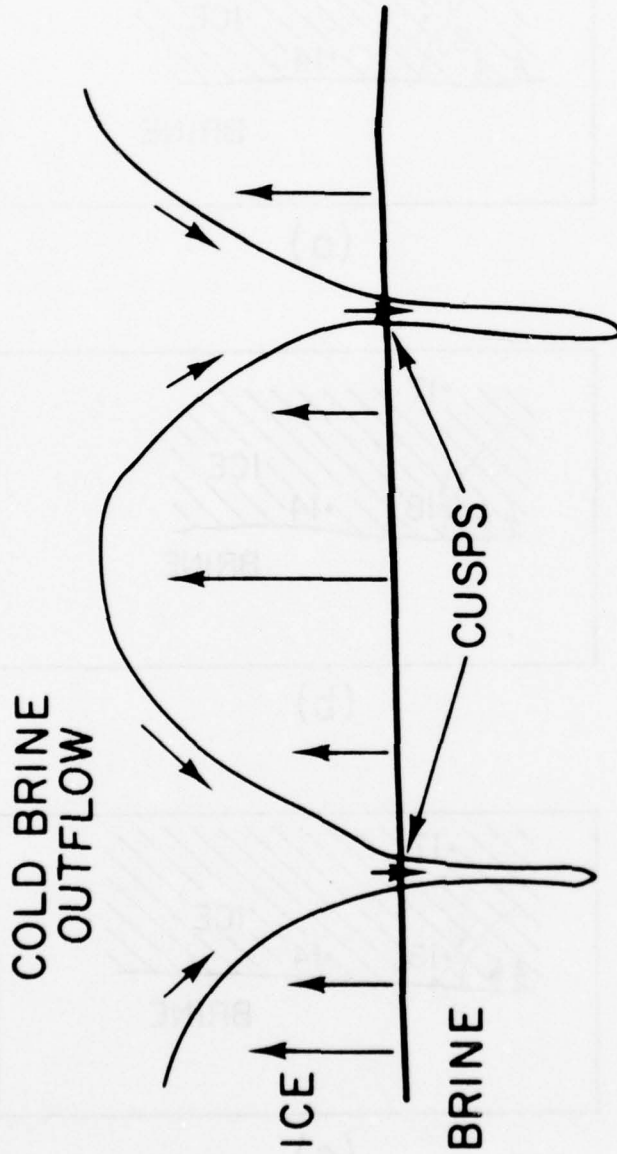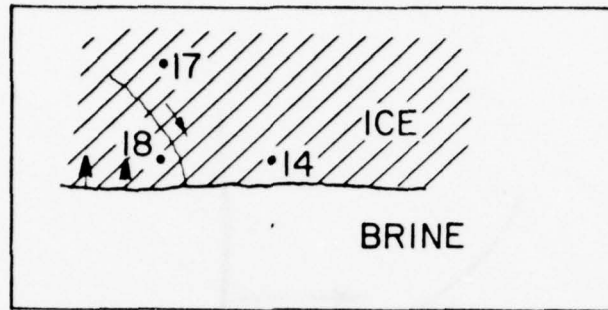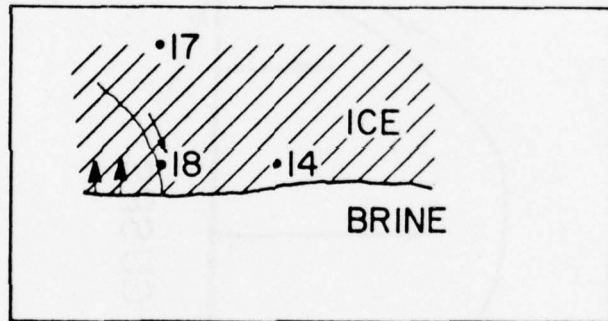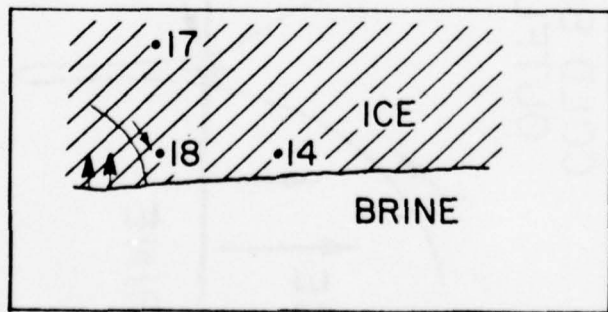
FIGURE 9. Idealized drawing of brine entering the skeleton layer and the cusplike outflow of denser brine. Cusps are usually separated by 10 mm.

FIGURE 10. Illustration of an observed sequence where a brine cusp flows through a thermocouple; (a) 0 min, (b) 5 min, (c) 10 min. See text for discussion.

a uniformly colored dye in its wake, so only the leading left edge of the cusp is visible. A comparison of the temperature records of 18 with 17 and 14, given in figure 11, shows that a 5×10^{-2} degree cold spike occurred as the cusp passed 18 at point b. Since the thermocouples above (17) and to the right (14) of 18 have no similar events, the disturbance is very likely caused by the cusp. Assuming a linear temperature gradient in the ice, the isotherms were displaced downward .5 mm by the flow associated with the cusp. Comparison of figures 9 and 10 shows that 18 is initially in a region of warm, upflowing seawater. As the cusp sweeps by, the temperature drops due to the cold, salty outflow, and then increases as presumably another upflow region passes the probe.

In a second experiment, a very regular set of cusps formed as dye reached the lower ice interface. Figure 12 shows the dye shortly after it entered the ice. After 20 minutes, a set of three streamers located under probes 3, 4, and 11 was still pouring dyed brine into the water. By 30 minute the plume under probe 4 was not visible, and those under 3 and 11 were weaker. The temperature record displayed in figure 13 show that probe 4 ceased cooling at point A (32 minutes) and by point B (36 minutes) its temperature had risen .065 degree. It then started to cool at a rate that was about the same as the other probes. From the photographs, it appears that fresh brine was flowing upward between the cusps. Figure 12 suggests when the cusp near probe 4 stopped flowing at about point A, the other cusps on either side of it maintained their flow and caused warmer water to flow up past probe 4. This caused the warm spike, shown between points A and B in the temperature record of 4. Once the brine enters the ice and stops flowing, it loses heat to its surroundings. This results in the cooling
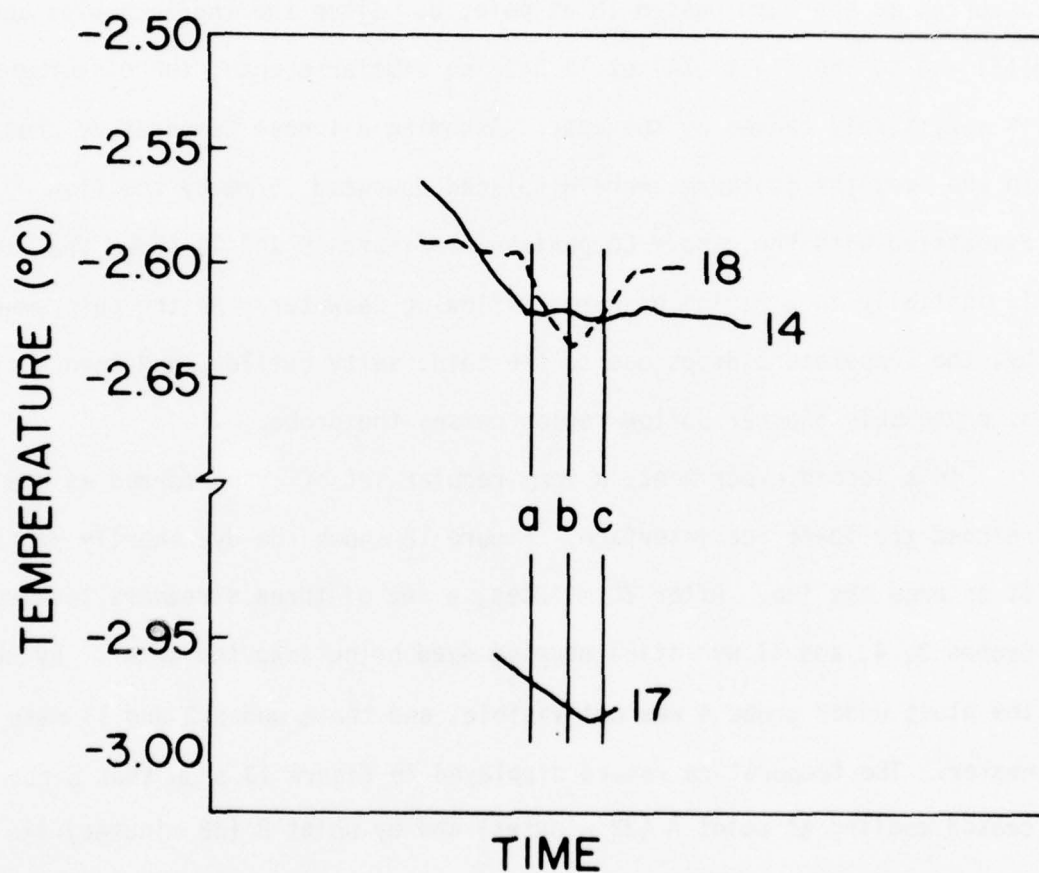
FIGURE 11. The temperature record for the sequence shown in figure 10.
a, b, c separated by 5 minutes.
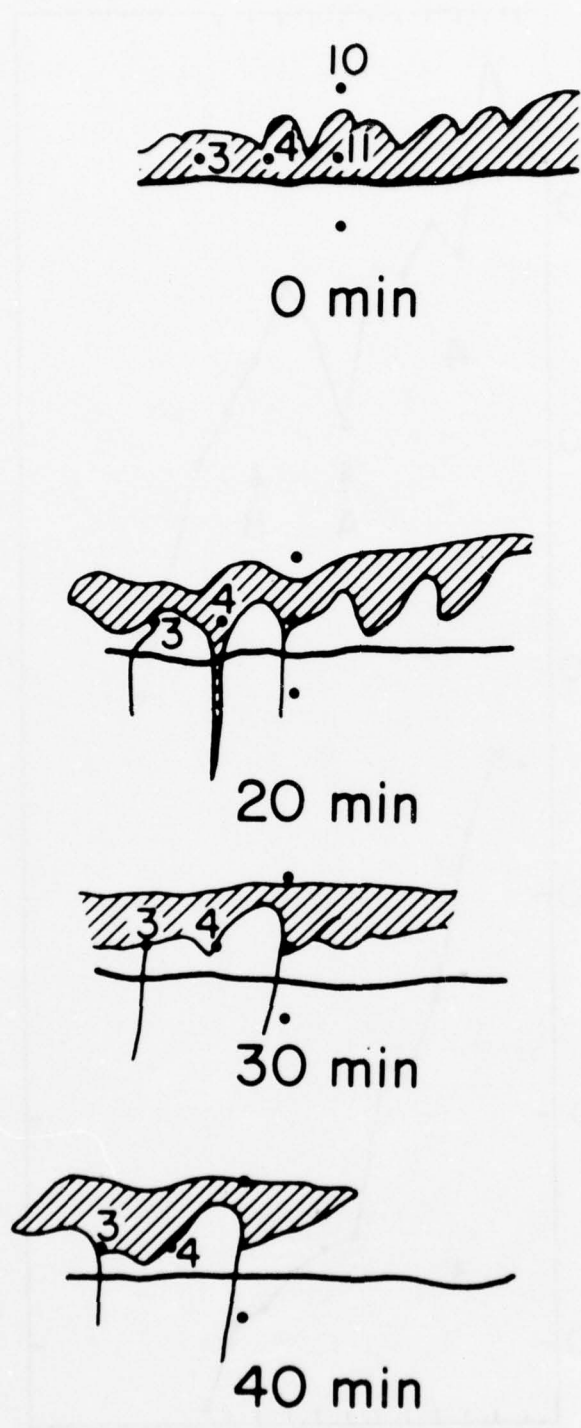
FIGURE 12. A sequence of 4 illustrations showing brine (a) going into the ice, then (b) cooling down and being ejected, and (c and d) one of the cusps stopping its flow. See text for further discussion.
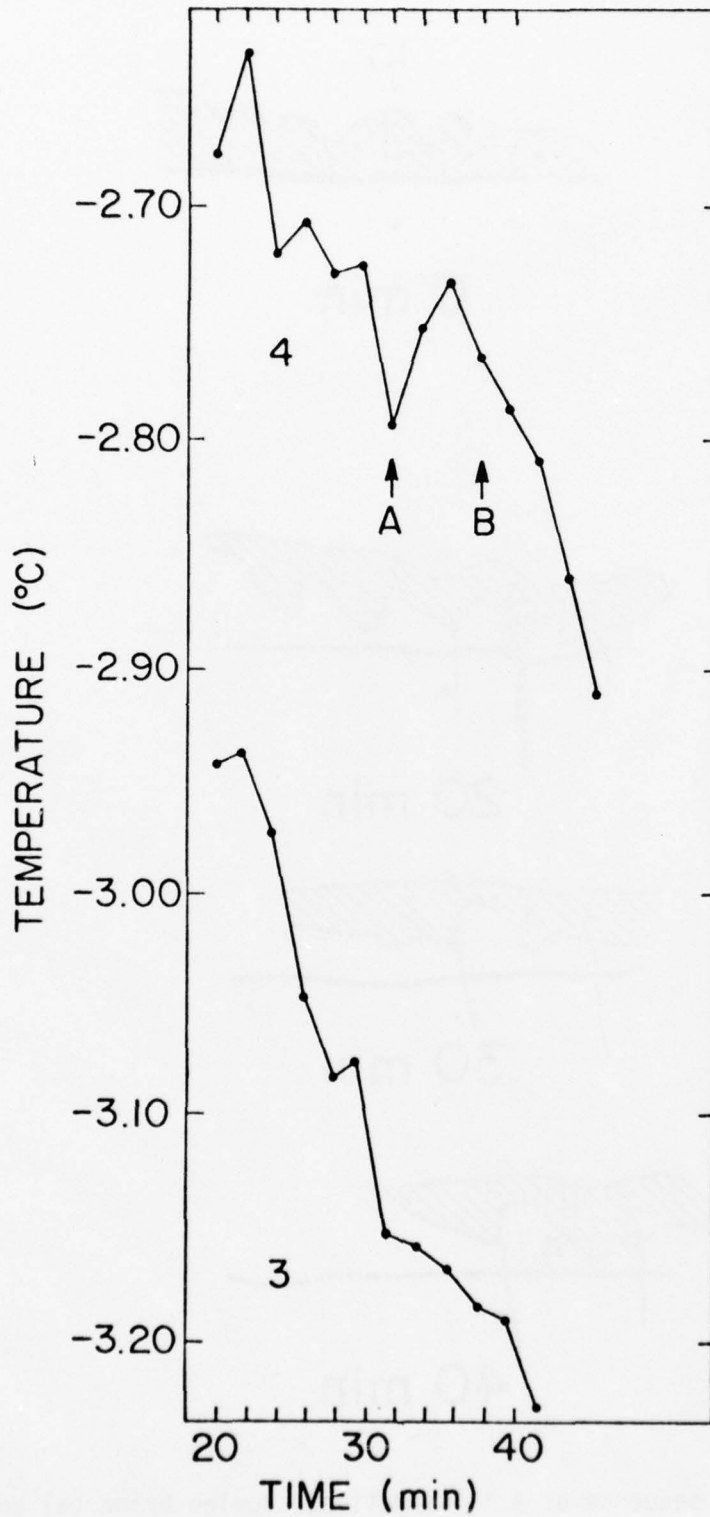
FIGURE 13. The temperature records from 2 of the probes in figure 12.

rate at probe 4 after point B returning to the value it had before the
intrusion at point A. In summary, these observations show that both
active convection and detectable temperature fluctuations occur in the
skeleton layer of the ice.

5. BRINE CHANNELS

5.1 General Observations

In the ice above the skeleton layer, a frequent and prominent feature
of our laboratory ice is the formation of brine channels. These are also
important in natural sea ice since they are probably the primary drainage
mechanism. Lake and Lewis (1970) give excellent examples of brine channels.
From their field observations in February and March, they report a density
of one large brine tube with a diameter greater than 1 mm per 180 cm^2 in
1.6 m thick ice. They also reported small tubes with diameters less than
1 mm, the average being 0.4 mm, at a height of 10 mm from the ice interface
with a density of 42 tubes per cm^2. This yields a brine channel volume of
about 5% of the total ice.

In other field investigations, Bennington (1967) observed one large,
open channel per 800 cm^2 for 0.2 m thick ice, with other frozen-shut
channels visible. In our experiments, once the ice reached 40 mm thickness,
there were one or two channels with diameters of the order of 1 to 3 mm
and lengths of 10 to 30 mm. The area covered by brine channels was traced
from photographs and then measured. Sometimes no channels were evident,
but usually the channels occupy 3% of the total area, which compares
favorably with the 5% observation of Lake and Lewis.

Figure 14 gives a typical sequence of an ice interface advancing into
the water and developing a brine channel. Dyed brine is being incorporated
into the ice in frame a. The brine channel marked by "α" is already quite
well-developed. A second brine channel, "β", develops within the next hour
and is visible in frame b. It appears to have developed from the vertical
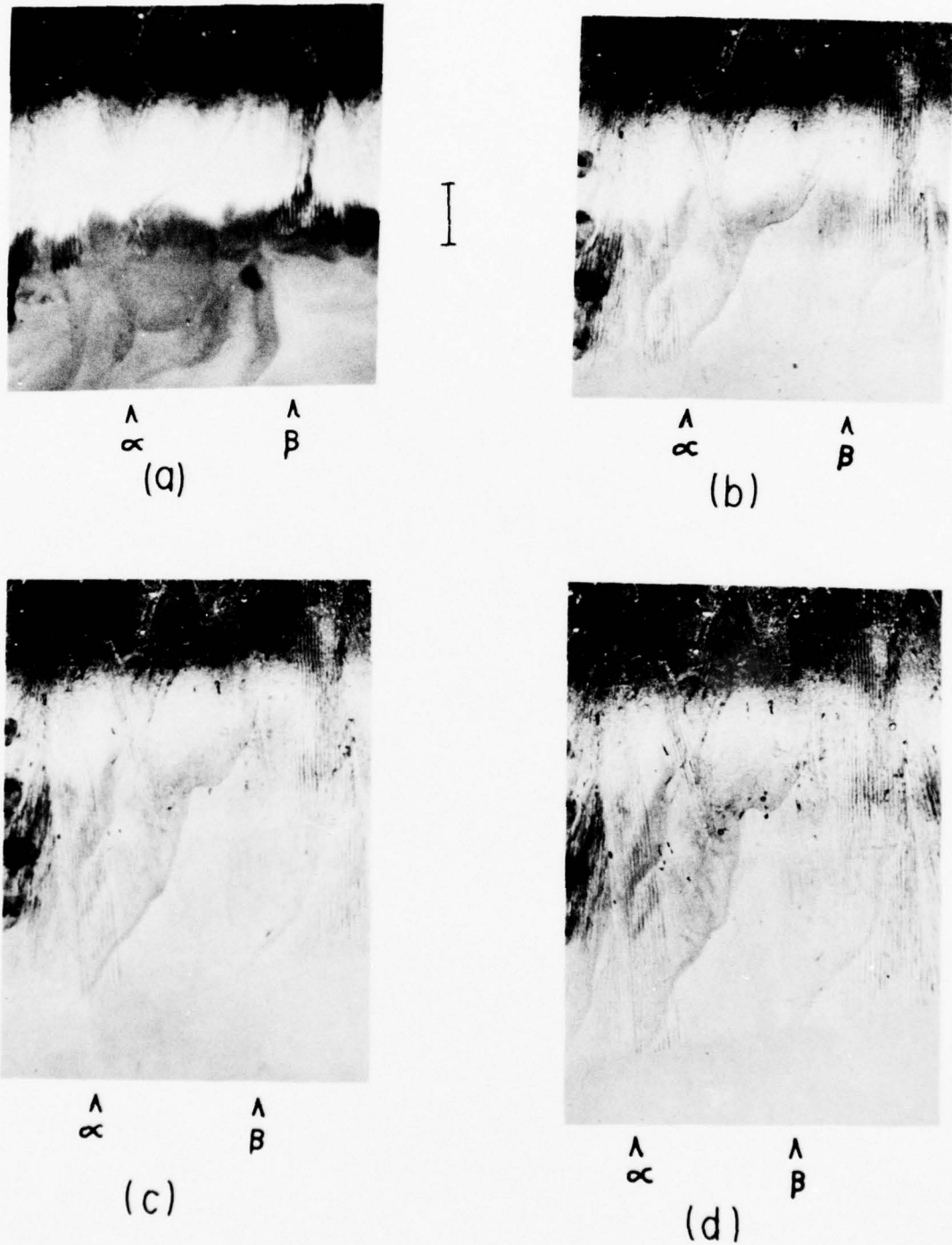
FIGURE 14. A sequence of 4 photographs showing the growth of typical laboratory sea ice; (a) 0 hours, (b) 1 hour later, (c) 2 hours later, (d) 3 hours later. Line to right of 14a is 10 mm in length. Dye has just reached the ice interface in 14a and the channels develop in later photos.

crystals immediately above it. The channels continue their development
in frames c and d, with air pockets visible in the interior of the ice
in the last frame. The air pockets are caused by dissolved air in the
brine coming out of solution as the brine freezes.

As figure 14 shows, the laboratory channels generally were not
vertical, but slope between 30° and 60° to the vertical. Similar angles
are reported in natural sea ice; for example, Lake and Lewis (1970)
observed numerous channels with angles of 40° to 54° feeding into a large,
vertical channel in their 1.6 m thick ice. Figure 15 is an unpublished
photograph from their 1968 field observations that shows brine channels
near the ice interface. This is especially interesting because it shows
a horizontal section of channel at "γ", which is similar to the horizontal
section of channel in the upper portion of channel "α" in figure 14d. There
is also a general resemblance in the slopes between the field ice of
figure 15 and the laboratory ice in figure 14. Martin (1977) also observed
channels in the ice interior with angles of about 45°. The same pattern
of vertical crystals and sloping brine channels that is present in our
ice is present in his field observations. The strong similarity between
the laboratory ice and the field ice suggests that our laboratory results
apply to the natural environment.

In the cases which we have studied, the isotherms in the ice are not
horizontal, but slope from 0° to 13°, with the average angle being 6°.
This can be checked against field measurements of the ice interface tilt
since isotherms near the ice bottom are parallel to the interface. Lewis
(1967) observed that the ice bottom was not smooth, but had many irregular-
ities, with slopes of 7° quite common, so that our laboratory slopes are
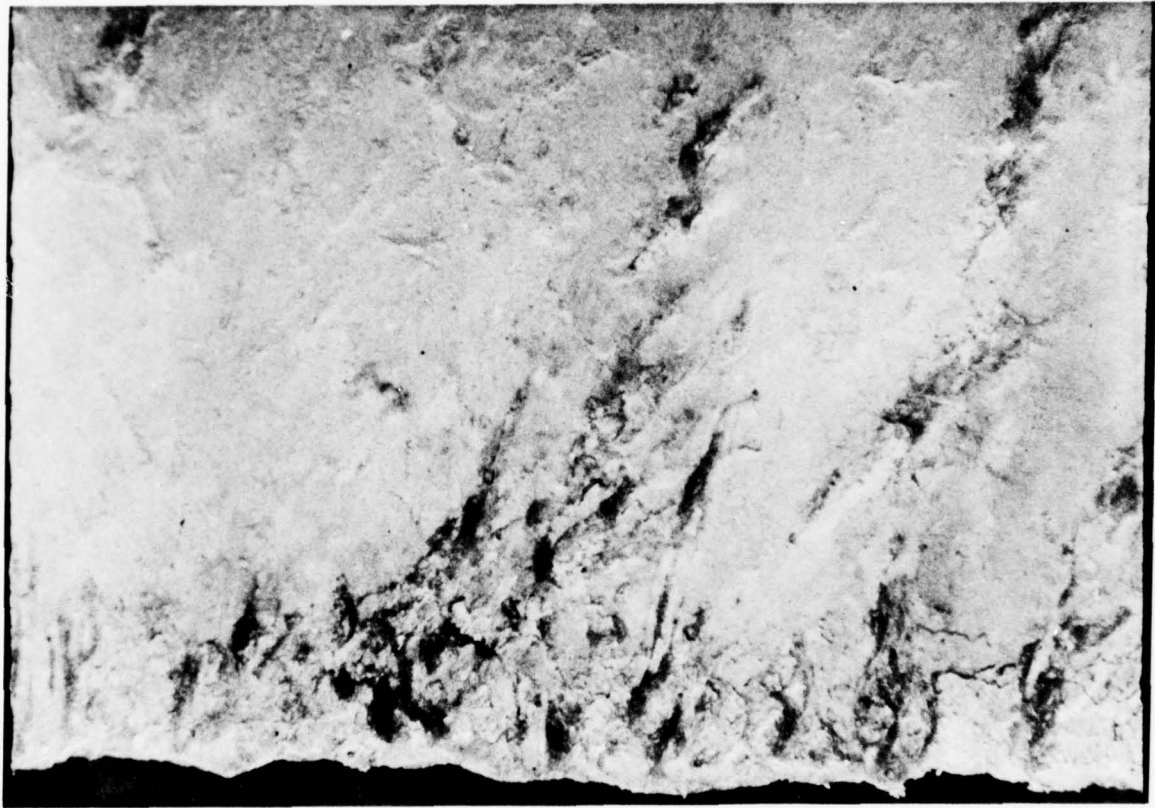
FIGURE 15. Side view of natural sea ice which shows tilted brine channels; previously unpublished photo from Lake and Lewis (1970).

of the same order as these field observations. Both our experiments and
Lewis's observations suggest that an isotherm tilt of only a few degrees
is associated with a brine channel slope of 30° to 60°. We also observe
that brine channels tilt in the same direction as the isotherms, which
means that at any horizontal level, the brine channels slope toward the
coldest region of the ice. Figure 16 is an example of this; the coldest
region is in the center of the array in 16a and the channels on either side
of the array slope toward it. Three hours later, 16b, the coldest region
of the ice, marked by the ice being thickest, has moved to the other side
of channel "δ". In response, the brine channel slope reversed its orienta-
tion and tilts to the left. This observation allows the isotherm pattern in
natural sea ice to be established by observing the brine channel tilts.
Figure 17 illustrates the brine channels found by the author in a newly
formed piece of ice at the edge of an arctic lead in February 1976. In this
ice, the thickest regions are the coldest regions, and the brine channels
all slope toward the thicker regions.

Because brine is originally trapped between ice crystals, we expect that
the brine feeds into the channels at the crystal boundaries which the channels
cut across. We observe this potential for feeding in many cases, (e.g. figure
14), which suggests that these crystals are a source of brine which starts
the channels. However, when viewing the formation of brine channels, they
often just seem to fade into existence in a photographic sequence (figure 14a,
b), their boundaries initially being ill-defined. This is because of limita-
tions in the photographic technique. When the camera had a field of view large
enough to see entire brine channels, resolution was not great enough to observe
brine pockets. When resolution was small enough to observe brine pockets, the

FIGURE 16. Two photos of brine channels. (a) has coldest region in center of thermocouple array; (b) has coldest region to left of channel, 3 hours later, and channel has changed direction of tilt at bottom. Black dots are thermocouples. The irregular blotches are silicone rubber spacers for the vacuum cell and are outside of the ice tank. Black "+" in upper right corner is a focusing mark for the camera. 5 mm spacing between thermocouples.

(a)
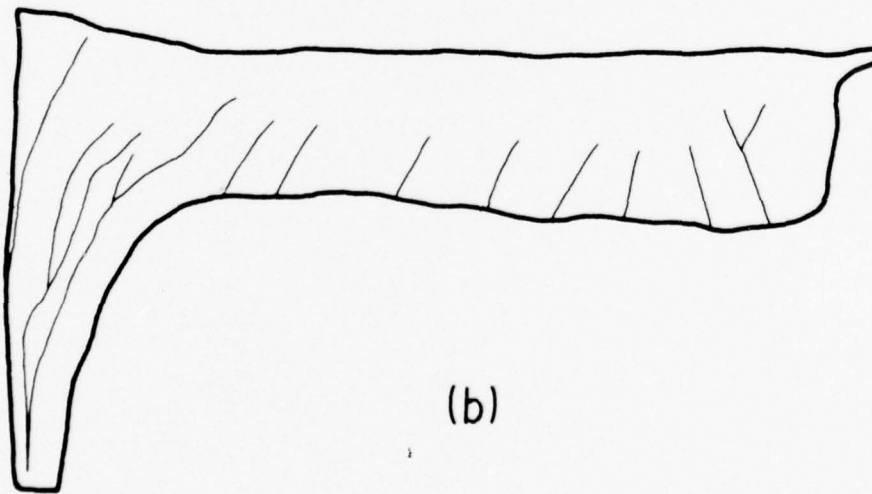
(b)

FIGURE 17. A piece of young sea ice, 100 mm thick, removed from a recently opened lead. (b) is a sketch of the brine channel pattern in the ice obtained by rubbing dye onto the ice.

brine channels were either too large to appear related to small features, or they were not present in the vicinity of the small features.

Another feature of brine channels is that when the brine drainage slows, or when a channel migrates, refreezing occurs in its wake. Figure 18 shows a refreezing channel that has many ice crystals growing in it. Figure 19 shows two photos separated by 3.5 hours showing a brine channel before and after it closes off. Once the region refreezes, brine channel movements in that region cease, which marks the conclusion of the role of brine channels in the desalination of cold, young sea ice.

5.2 Convection in Channels

In several experiments, brine did not flow unidirectionally out of the ice, rather we observed convection in the channels. Our observations divide into two categories; convection caused by dyed fluid entering the ice and spontaneous convection in the ice interior. In the first category, wherein the greatest number of observations occurred, the injected, dyed water flowed up into the brine channels simultaneously with downward flow of dense brine. For tilted channels, the clear dense brine flowed down the lower side of the brine channel, and the dyed, fresher brine flowed up along the upper wall.

When a sharp boundary existed between the dyed and undyed water, we were able to measure the rate at which the seawater rose into the ice. Figure 20 is a series of illustrations taken from photographs at the mouth of a brine channel. The channel width was 1.4 mm and typical velocities were 0.25 mm s^{-1} out of the channel. These measurements imply a volume flux of 0.38 mm^{3}s^{-1} up the channel. To calculate the heat flow into the

FIGURE 18. Brine channel tnat is freezing shut; note the random
crystals that fill the channel. Distance between
horizontal lines is 10 mm.

(a)

(b)
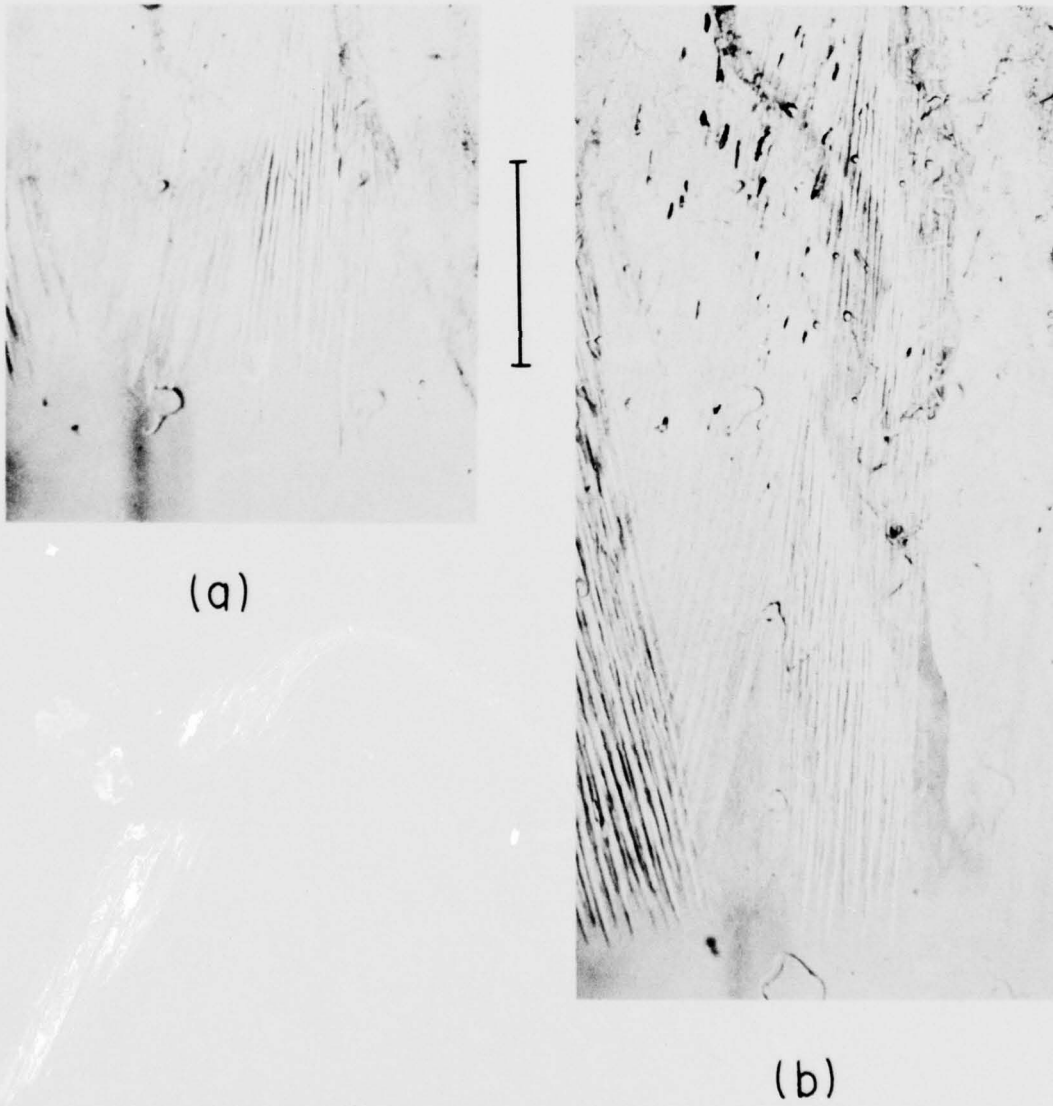
FIGURE 19. A brine channel (a) developing in the ice and (b) after it has frozen shut 3.5 hours later. Line to right of 19a is 10 mm in length.
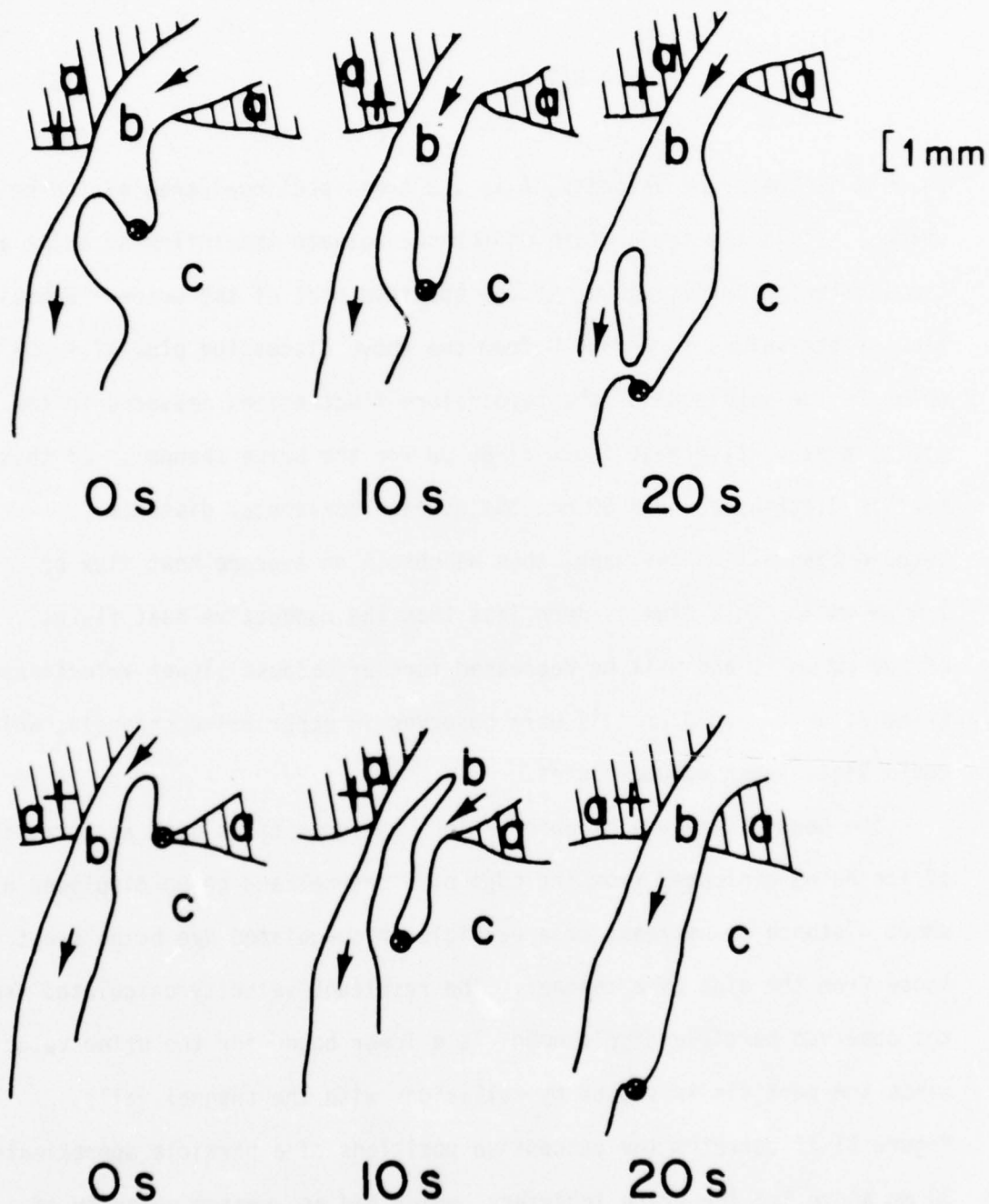
FIGURE 20.   Illustrations of two sequences of movement of brine at the
             ice-brine interface. The '●' marks a particular brine parcel.
             The '+' is a fixed reference position on the tank walls.
             10 sec between frames; (a) ice, (b) outflowing brine, (c) water.

ice, we use

$$F = A U \Delta T c_p \rho , \qquad (5)$$

where U is the brine velocity, A is the cross-sectional area of the brine channel, ΔT is the temperature difference between the inflowing brine and the outflowing brine, and c_p is the specific heat of the brine. Substitution of the values for A and U from the above discussion plus $\Delta T = .05°C$, which is the magnitude of the temperature fluctuations measured in the ice, yields a convective heat input of 80 μW for the brine channel. If this heat is distributed over 50 mm, the average horizontal distance between channels in our tank, then we obtain an average heat flux of 1.6 μW mm^{-1}. This flux is much less than the conductive heat fluxes of 200 μW mm^{-1}, and will be decreased further because slower velocities (from 35 μm s^{-1} to 6 μm s^{-1}) were observed in other brine channels, which would yield lower volume fluxes.

The second category of observations includes cases such as a crystal of ice being dislodged from the edge of a channel and being displaced a short distance downstream, or a particle of coagulated dye being swept loose from the side of a channel. The resultant velocity calculated from the observed particle displacement is a lower bound for the brine velocity since the particle is slowed by collisions with the channel walls. Figure 21 illustrates the successive positions of a particle approximately 30 mm above the ice-brine interface, which had an average velocity of 44 μm s^{-1} during the 70 seconds that it was observed moving.
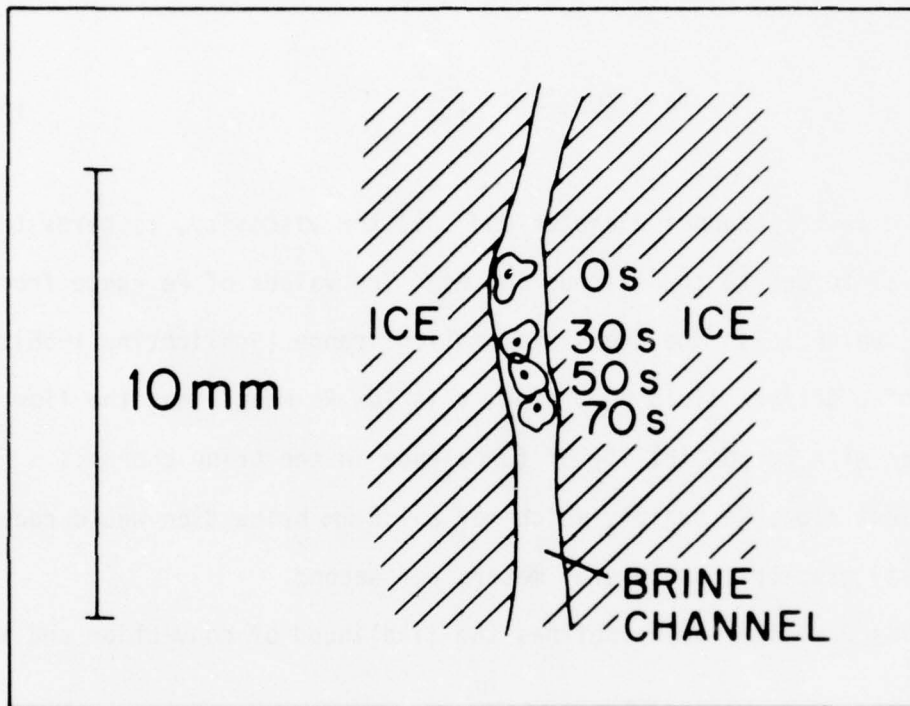
FIGURE 21. Illustration of the movement of a dye particle in a
brine channel. The dot marks the center of the dye
particle. Time in seconds.

At least two nondimensional numbers describe the interior flow; namely the Reynolds number, Re, and the Rayleigh number, Ra. The Reynolds number for these flows, calculated from

$$Re = (Ud) \; \nu^{-1} \quad , \tag{6}$$

where d is the channel diameter and ν is the viscosity, compares the inertial forces to the viscous forces. The values of Re range from 0.2 to 0.005, which is in the "very slow motion" range (Schlichting 1968). For flow of a uniform fluid in a pipe, this low Re means that the flow will be laminar with no possibility of turbulence in the brine channels. For turbulent flow, Re >> 10^4, which for a 1.5 mm brine tube would require a velocity greater than several meters per second.

The Rayleigh number defines the likelihood of convection and is given by

$$Ra = (\rho D\nu)^{-1} \frac{d\rho}{dz} \; g \; r^4 \quad , \tag{7}$$

where r is the tube radius, D is the salt diffusivity, ν is the viscosity, and g is the gravitational acceleration. For a cylindrical tube, convection occurs for Ra greater than 68 (Wooding 1959). If we consider the brine and ice to be in equilibrium in the interior, then the temperature T, will determine the salinity. Cox (1974) states that the best available equation of state for the brine in a NaCl brine-ice system in equilibrium is

$$\rho_{brine} = 1 + 8 \times 10^{-4} \; S, \tag{8}$$

where $\quad$ S = -17.5730 T - 0.381246 T^2 - 3.28366 x 10^{-3} T^3 . $\qquad$ (9)

Combining equations 7-9 with $\frac{dT}{dz}$ = 0.06 deg mm^{-1} and T = -4°C, convection can occur in a tube with a radius greater than .4 mm, which is the radius of the larger brine channels. In summary, the brine channel flow is subcritical with respect to Re and either subcritical or supercritical with respect to Ra.

5.3 Movement of Brine Channel Walls

In the tank, brine channels migrate both horizontally and vertically through sea ice. They move by melting one wall, the lower wall if the channel is not vertical, and freezing ice to the other wall. Our observed brine channel migration rates vary from zero to 1.6 μm s^{-1}, with the majority of the moving channels traveling at a speed from 0.1 to 0.6 μm s^{-1}. The cooling rate of the ice, the horizontal temperature gradient, and the vertical temperature gradient were measured for five of the experimental runs in which brine channel migration occurred in the vicinity of the temperature-probe array. Figures 22-24 are graphs of brine channel velocity versus cooling rate, horizontal temperature gradient, and vertical temperature gradient. From the scatter of the data points, it is evident that none of these quantities singly control the channel velocity. However, it is significant that the brine channel walls always melt toward the warmer side, as shown in figure 23 by all the data points lying in the first quadrant.

If the channels moved because of the conductive heat flux in the ice, we would expect the wall velocity to increase as the cooling rate or the temperature gradients increase. Since this relation is not verified by
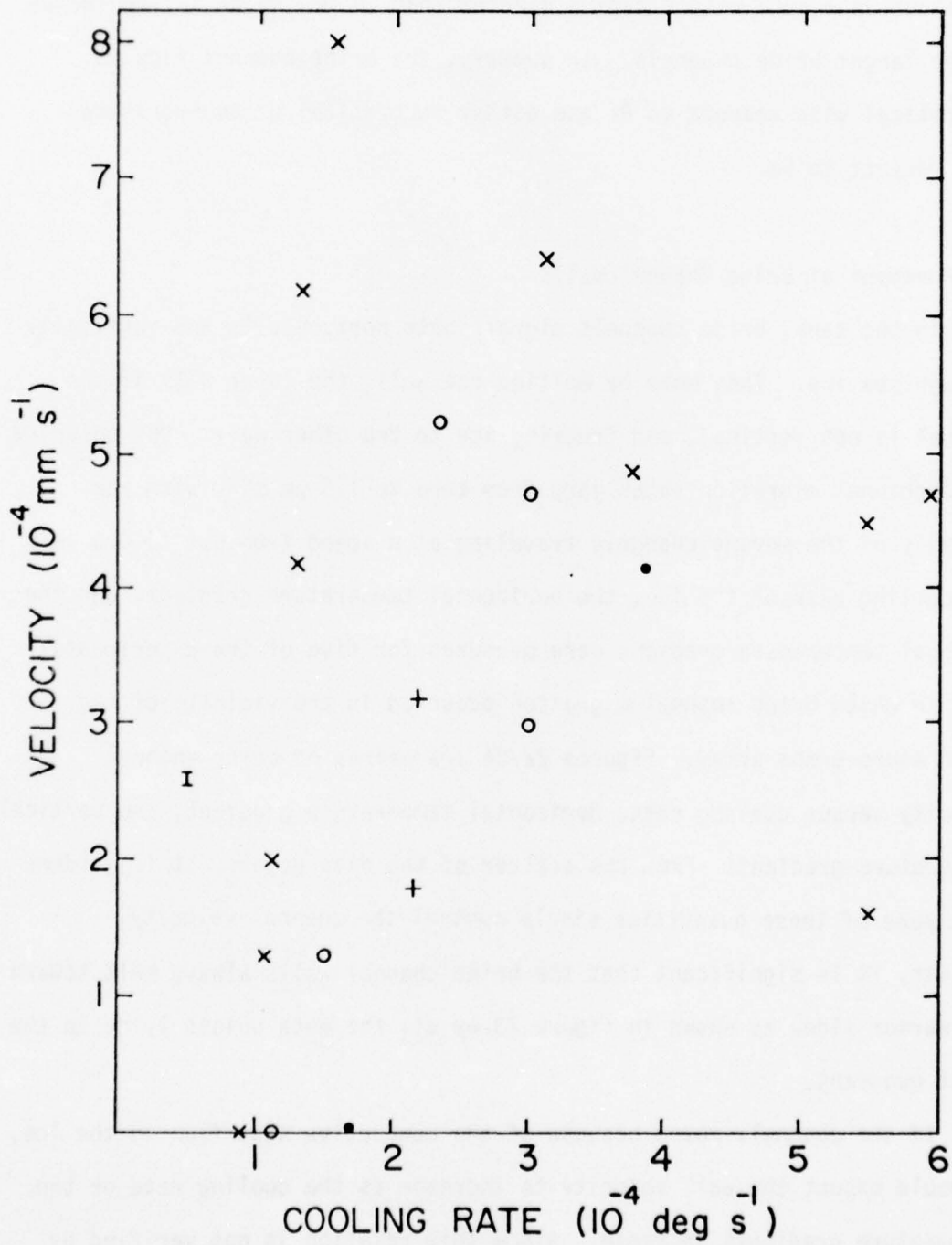
FIGURE 22. Plot of cooling rate versus velocity of a brine channel wall for 5 experimental runs.

- 50 -
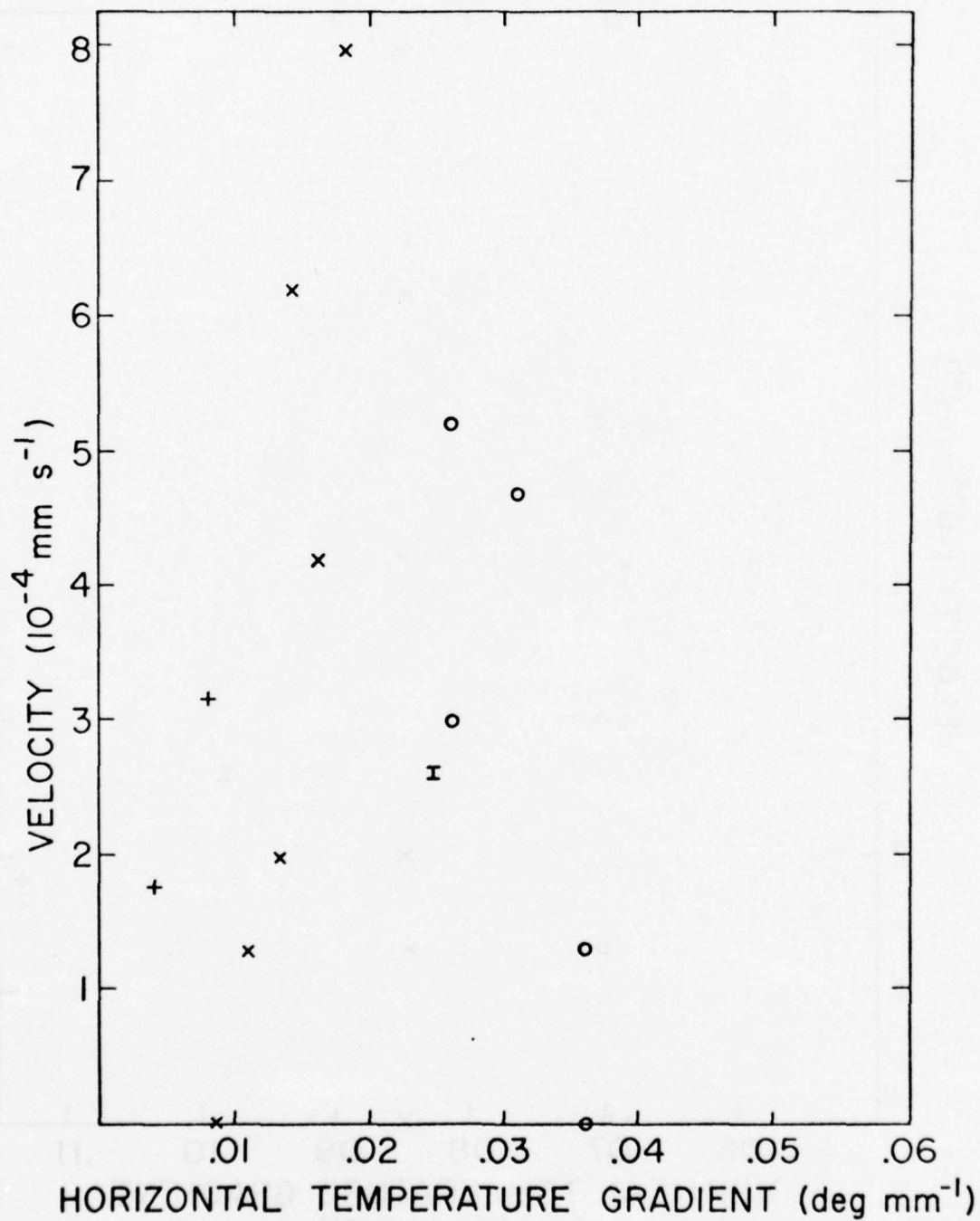
FIGURE 23. Plot of horizontal temperature gradient versus brine channel
wall velocities for 5 experimental runs.
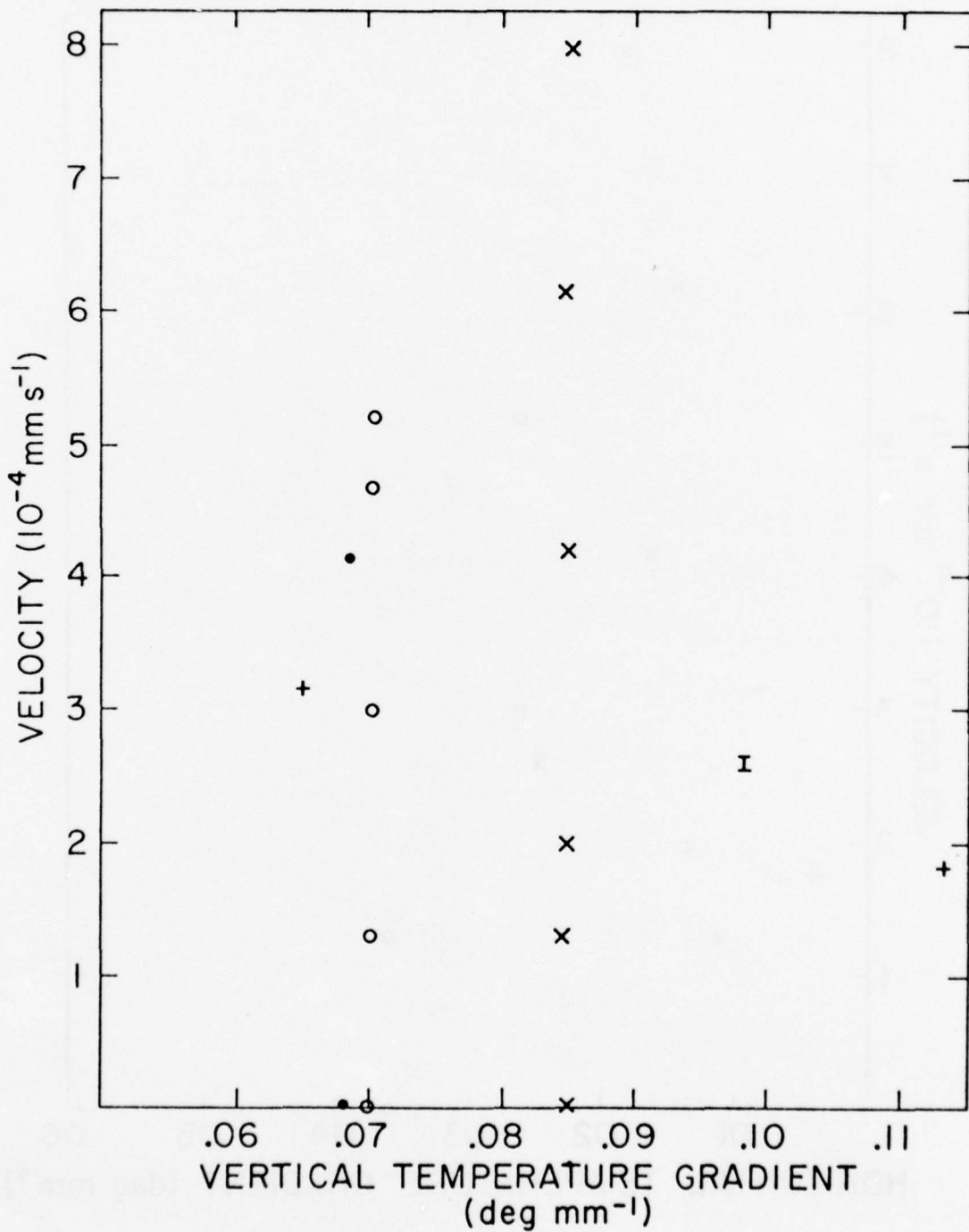
FIGURE 24. Vertical temperature gradient versus wall velocities for 5 runs.

the data, convection in the brine channel is the only mechanism left as the cause of the wall motion.

The criteria for convection, Ra, is a function of T and $\frac{dT}{dz}$ in addition to r, the channel radius. It would have been desirable to plot Ra against the wall migration rates to show that convection causes the migration, but the uncertainties in determining r do not allow the direct evaluation of Ra in most of the cases for channel wall migration. As a weaker alternative, we compare estimates for brine velocities with ice melting rates to see if convection can provide the heat fluxes required for the wall movement.

Consider a vertical brine channel with a diameter of 1.4 mm. The amount of heat needed to melt the channel walls can be calculated with the aid of equation 1. Typical channel melt rates of 1 μm s^{-1} to 8 μm s^{-1} will yield latent heat fluxes of 42 μW mm^{-1} to 338 μW mm^{-1}. To compute an upper limit on the amount of heat that can be supplied by brine channel flow, consider the following model. Suppose the brine in the channel has the same linearly decreasing temperature profile as the surrounding ice. Then the brine will be unstable since density increases with height, and convection will eventually occur if Ra>68. If laminar flow starts in the channel, the brine with its linearly decreasing temperature will flow down the tube. The flow will transport the temperature gradient and produce a convective heat flux per unit length given by

$$F_c = A U \ \frac{dT}{dz} c_p \rho \tag{10}$$

where dT/dz is the vertical temperature gradient. For a vertical gradient of 0.08 deg mm^{-1} and U = 0.25 mm s^{-1}, F_c = 129 μW per millimeter of channel.

This number is in the middle of the range for latent heat fluxes, so convection could drive the lateral wall melting.

5.4 Temperature Variations

When a brine channel sweeps past a thermocouple, the temperature changes. In one instance, a very active brine channel swept across several temperature probes in the square portion of the probe array. Figure 25 shows two photographs of the channel at different times as it passes through the array, and figure 26 is a schematic of the channel during its entire traverse of the array. Other channels having a comparable displacement were photographed outside the temperature array during other runs, so channel movements of this scale were fairly common.

Figure 27 shows the temperature record of the array, where the temperatures are given at four different depths and times, with each horizontal level of probes being arranged in a vertical column so that the brine channel movement across each level can be readily seen. At the top level, the channel only moved slightly and remained closest to probe 6, which always had the coldest temperature in the ice. At the second level, the channel moved a horizontal distance of 10 mm, going from probe 13, past 7 to 1, the coldest temperature always being measured by the probe that was closest to the brine channel. The temperature of the probes nearest the brine channel stayed between 0.05 to 0.01 degrees colder than the other probes at that level. At the next lower level, there was a 0.06 degree drop in temperature as the channel moved from probe 14 to 8. Finally, at the bottom level nearest the ice interface, the temperature between probes

(a)

(b)

FIGURE 25. Photographs of a brine channel as it passes through the temperature array. b is 2 hours after a.

FIGURE 26. An illustration of the channel from figure 25 for its
entire period of movement; —, 0 hours; --, 0.5 hours;
•—•, 1.0 hours; x-x, 2.0 hours; o-o, 3.0 hours;
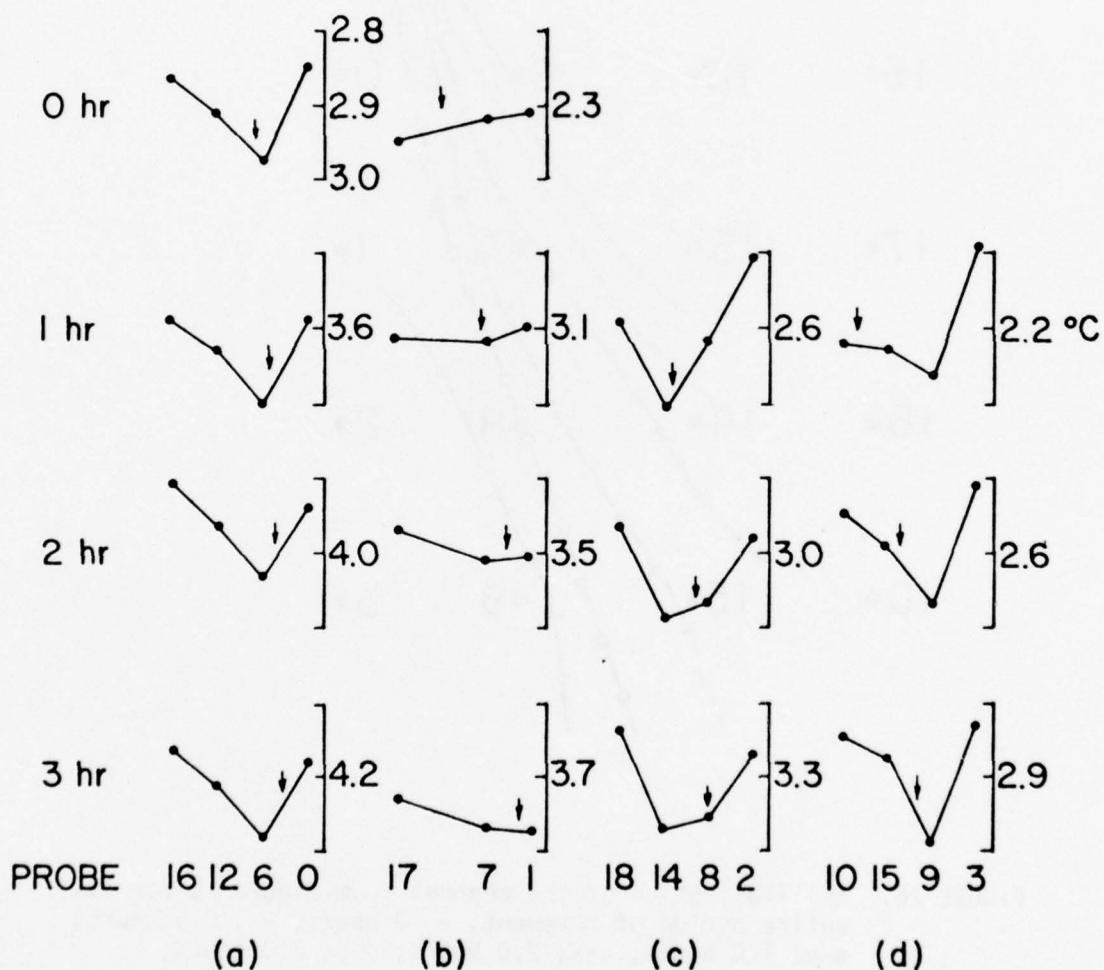++, 4.0 hours.

FIGURE 27. The temperature records for the period given in figure 26: (a) top level, (b) 5 mm down from top, (c) 10 mm down from top, (d) 15 mm down from top. Probe numbers are given at the bottom of the columns. At all levels, the temperature increment is 0.1°C between marks. The arrow marks the position of the brine channel.

changed almost 0.1 degree a's the channel moved from probe 10 to 9.
During this run, a calibration error may have caused the third and bottom
levels not to indicate that the probe nearest the channel was always colder.
In spite of this error, a consistent pattern of the temperature dropping
as a channel swept by a probe emerges from the figure.

Temperature changes also occurred when convection starts in a brine
channel. Figure 28 shows two ice photographs separated by a ten minute
interval. The prominent brine channel labeled "ε" has no signs of convection
in 28a, but in 28b a plume of dye is emerging from the channel into the
brine below the ice. After the flow began, the probe located 6 mm above
the ice interface where the channel empties into the underlying water
increased its temperature relative to another probe at the same level by
about .1°c. This temperature increase supports the convective overturning
theory that there is an upflow in the brine channel at the same time that
an outflow occurs. An upflow brings warmer brine into the ice, so that the
temperature adjacent to the upflow will increase.

The model we propose for brine channel convection and wall migration
initially has brine at rest in the channel. When Ra exceeds its critical
value, convection starts with a descending plume of cold, dense brine
flowing down the lower side of the nonvertical channel. A replacement
flow of warmer, less-saline brine flows up the high side. This flow is
accompanied by a cooling on one side of the channel and a warming on the
other side, which disturbs the temperature gradient in the ice. There
will also be a heat flux from the warm upflow to the colder downflow. If
the tube is slanted, this heat flux causes freezing on the upper wall and

FIGURE 28. Two photos of ice showing brine channel ε before (a) and
after (b) brine starts flowing out of it. Photos separated
by 10 minutes.

melting on the lower. As the system tries to reach equilibrium, the eutectic condition (equation 9) contributes to melting on the lower wall since the salty brine must be diluted as it flows down the ice wall into a warmer region, and melting is the only source of fresh water for dilution. Another source of heat for the brine channel walls is the mean ice temperature gradient. The isotherms in young sea ice are often not horizontal (section 5.1). One effect of this upon the brine channels, which slope in the same direction as the isotherms, is that the heat flux per-unit-length of the channel is increased, which will increase the melting rate of the channel. All of these effects work to melt channel walls whenever there is convection in the channel. After convection stops, the horizontal temperature gradient will dissipate. The vertical gradient in the ice will be established in the brine and eventually the brine in the channel may become unstable and start flowing again. This process will continue until the channel radius becomes too small for convection to occur.

6. SMALL SCALE ICE FEATURES

When brine channels are not present, or when a channel begins to freeze shut and convection is no longer present, the small scale features of sea ice become significant. During two experiments, microphotographs were taken by focusing the camera on a 10 mm by 8 mm section of ice. In both cases, brine tubes and brine pockets were present and the formation of brine pockets from brine tubes was documented.

6.1 Brine Tubes

Brine tubes are cylindrical brine-filled hollows in the ice which are closed at one end with a bulb-like cap. In our case, the tubes are 0.4 mm long with a diameter of 0.1 mm (figure 29). These tubes have the same diameter as tubes reported by Lake and Lewis (1970), but our tubes are shorter than the field observations of 20 to 30 mm.

Brine tubes could be important to the dynamics of brine channels. To examine brine tubes as a brine source for driving brine channel convection, consider what happens as a tube freezes shut. The time-averaged brine velocity through the tube entrance will be 0.1 times the tube length divided by the time it takes to freeze shut. We observed that the tube in figure 29 took two hours to freeze shut, so the brine moves out of the tube at a velocity of 5.5 nm s^{-1}. Since it is so slow, it will not cause any temperature disturbance. This velocity is over 1000 times less than the slowest observed convective flow of 6 μm s^{-1} in the brine channel.

An estimate of the brine velocity in a channel due to expulsion is obtained by assuming that all of the brine moves through a 1 mm^2 brine

FIGURE 29. Illustration of a brine tube pinching off into brine pockets. An actual photo is given in (b) for the situation one hour after (a); (c) is two hours after (a). (a) and (c) have the same scale; (b) is smaller.

channel. If we assume that the channels are spaced 50 mm apart and have a conical-shaped drainage area, then in 40 mm deep ice each channel has a drainage volume of 1600 mm^3. If 10% of this is brine volume, and half of it freezes in 2 hours, then the volume expelled will be 10% of the brine volume frozen, or 8 mm^3. This implies a steady velocity of 1.1 μm s^{-1} through the channel.

Another source of brine for the channel could be gravity drainage from the ice rising above the water level due to buoyancy. The brine would come from intercrystalline channels which have one end open to the air while the other feeds into a brine channel. This does not happen in my experiment because the ice is frozen to the tank walls and cannot float. We therefore will examine this process to estimate its importance in natural sea ice. If the ice front is advancing at a rate of 3 μm s^{-1}, then the ice top rises above the water level at 0.3 μm s^{-1}. If 10% of the sea ice consists of brine in the small channels, a high estimate, then the drainage rate through a 1 mm^2 brine channel with 50 mm of drainage area at the top of the ice would be 2.4 μm s^{-1}. When this is combined with the expulsion velocity, it is still unable to account for the high velocities recorded in the brine channel. The observed channel velocities must therefore be due to the convective replacement of brine by seawater entering the ice.

6.2 Brine Pockets

A brine pocket is a bubble of brine, surrounded by ice, that has only limited, if any, communication with other brine masses. During both micro-photograph experiments, brine pockets were photographed forming from the freezing of brine tubes, which indicates that the transition occurs frequently.

Figure 29 shows a brine tube pinching off in a two hour period to form two brine pockets and a smaller brine tube (figure 29). These brine pockets, which are about 0.1 mm in diameter, are located in the interior of the ice, approximately 20 mm from the interface. The cooling rate was 85 μ deg s^{-1} and the vertical temperature gradient was .07 deg mm^{-1}. Small brine tubes of this diameter are very abundant at the bottom of natural sea ice (Lake and Lewis 1970). In the run illustrated in figure 30, which is very similar to the previous example, a brine tube pinched off over a 5 hour period. The entire region of sea ice was cooling at a rate of 6 μ deg s^{-1}, but the vertical temperature gradient was the same as the first case, .07 deg mm^{-1}.

Another important aspect of brine pockets is that as they freeze they cause a pressure increase in the ice, which is the mechanism behind brine expulsion. The pressure increase will distort the ice which will take the form of cracking along the ice crystals, slipping along crystal axis, or perhaps deformation of crystal structure. Since brine pockets are located originally at crystal boundaries, cracking may preferentially occur along the boundaries. However, the mechanism of temperature gradient migration may transport some brine pockets into a crystal, so cracking is not limited to crystal boundaries. Engineering measurements of the compressive strength of sea ice done by Peyton (1963) show that the strength is significantly lower for loads applied along the c-axis direction than for loads applied perpendicular to the c-axis direction. This suggests that cracks preferentially occur across crystals, which may account for brine channels cutting across crystals as in the upper portion of the channel in figure 25.

The cracking and expulsion produced by brine pockets cooling could be the cause of brine channels sloping toward the colder regions. Since brine
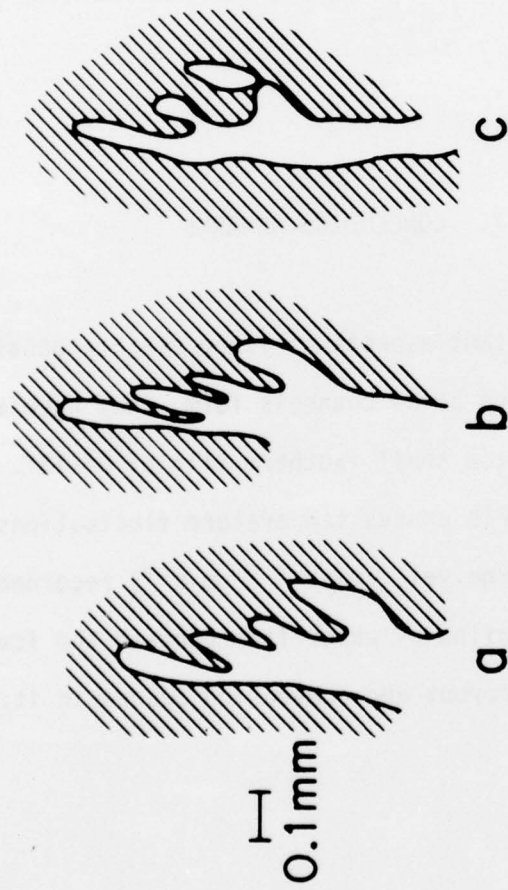
FIGURE 30. Another case of a brine tube forming a brine pocket over a period of 5 hours; (a) 0 hours, (b) 1 hour, (c) 5 hours.

channels transport brine from the interior of the ice, a channel should preferentially form where the supply of brine is the greatest, which is where the temperature changes the most. At any particular horizontal level, the temperature has changed the most where it is coldest. This suggests that brine channels slope toward the cold as they grow as a consequence of the amount of cracking and the availability of brine.

7. CONCLUDING REMARKS

There are four important aspects of young sea ice desalination found in this study. First, when brine channels form, they have a slope of 30°-60° in the same direction as the small isotherm tilt of 0°-13°. Second, convection in brine channels causes temperature fluctuations of the order of 0.05°C. Third, the large velocities (>6 μm s^{-1}) recorded in brine channels are fed by the inflow of water from beneath the ice. Finally, the skeleton layer is highly porous and convection occurs in it.

REFERENCES

Anderson, D. L. and Weeks, W. F. 1958. A theoretical analysis of sea-ice strength. Trans. Amer. Geophysical Union, Vol. 39, p. 632-40.

Bennington, K. O. 1967. Desalination features in natural sea ice. Journal of Glaciology, Vol. 6, No. 48, p. 845-57.

Brunner, W. and Batzer, T. 1965. Practical Vacuum Techniques. Reinhold Publ. Corp.

Carslaw, H. S. and Jaeger, J. C. 1959. Conduction of Heat in Solids. Clarendon Press.

Cox. G. F. 1974. Brine Drainage in Sodium Chloride Ice. [Ph.D. thesis, Dartmouth College, Hanover, New Hampshire.]

Cox, G. F. N. and Weeks, W. F. 1974. Salinity variations in sea ice. Journal of Glaciology, Vol. 13, No. 67, p. 109-20.

Dushman, S. 1949. Scientific Foundations of Vacuum Technique. Wiley.

Eide, L. and Martin, S. 1975. The formation of brine drainage features in young sea ice. Journal of Glaciology, Vol. 14, No. 70, p. 137-54.

Kaufman, D. W. 1960. Sodium Chloride. Reinhold Publ. Corp.

Lake, R. A. and Lewis, E. L. 1970. Salt rejection by sea ice during growth. Journal of Geophysical Research, Vol. 75, No. 3, p. 583-97.

Lewis, E. L. 1967. Heat flow through winter ice. In Physics of Snow and Ice, Vol. 1 (ed. H. Oura), p. 611-31. Institute of Low Temperature Science, Hokkaido University, Japan.

Lewis, E. L. and Weeks, W. F. 1971. Sea ice: some polar contrasts. In Symp. on Antarctic Ice and Water Masses (ed. G. Deacon), p. 28-38. Scott Polar Research Institute, University of Cambridge.

Malmgren, F. 1927. On the properties of sea ice. The Norwegian North

    Polar Expedition with the "Maud" 1918-1925. Scientific Results,

    Vol. 1, No. 5.

Martin, S. 1974. Ice stalactites: comparison of a laminar flow theory

    with experiment. Journal of Fluid Mechanics, Vol. 63, Pt. 1, p. 51-86.

Martin, S. 1977. The seasonal variation of oil entrainment in first year

    arctic sea ice: a comparison of NORCOR/OCS observations. Univ. of

    Wash., Dept. of Oceanography Special Report No. 71, 10 March 1977.

Neumann, G. and Pierson, W. J. 1966. Principles of Physical Oceanography.

    Prentice-Hall.

Peyton, H. R. 1963. Some mechanical properties of sea ice. In Ice and Snow

    (ed. W. D. Kingery), p. 107-13. M.I.T. Press.

Schlichting, H. 1962. Boundary Layer Theory. McGraw-Hill.

Untersteiner, N. 1967. Natural desalination and equilibrium salinity

    profile of old sea ice. Journal of Geophysical Research, Vol. 73,

    No. 4, p. 1251-57.

Weeks, W. F. 1976. Sea ice conditions in the arctic, AIDJEX Bulletin, No. 34,

    Dec. 1976, p. 173-96.

Wooding, R. A. 1959. The stability of a viscous liquid in a vertical tube

    containing porous material. Proc. Roy. Soc., A, Vol. 252, p. 120-34.

DISTRIBUTION LIST

CONTRACT N00014-76-C-0234
NR 307-252

DR G LEONARD JOHNSON
CODE 461
OFFICE OF NAVAL RESEARCH
ARLINGTON, VA   22217

DEFENSE DOCUMENTATION CENTER
CAMERON STATION
ALEXANDRIA, VA   22314 (12 copies)

OFFICE OF NAVAL RESEARCH
CODE 105
ARLINGTON, VA   22217 (6 copies)

DIRECTOR, US NAVAL RESEARCH LAB
CODE 2627
WASHINGTON, D C   20375 (6 copies)

COMMANDING OFFICER
CODE L61
NAVAL CIVIL ENGINEERING LAB
PORT HUENEME, CA   93043

DEPARTMENT OF THE ARMY
OFFICE, CHIEF OF ENGINEERS
ATTN DAEN-RDM
WASHINGTON, D C   20314

CHIEF OF ENGINEERS
ATTN DAEN-MCE-D
DEPARTMENT OF THE ARMY
WASHINGTON, D C   20314

COLD REGIONS RESEARCH & ENG LAB
P.O BOX 282
HANOVER, NH   03755

DR REID A BRYSON
INST FOR ENVIRONMENTAL STUDIES
UNIVERSITY OF WISCONSIN
1225 W DAYTON STREET
MADISON, WI   53706

LIBRARIAN
NAVAL ARCTIC RESEARCH LAB
BARROW, AK   99723

WOODS HOLE OCEANOGRAPHIC INST
DOCUMENT LIBRARY LO-206
WOODS HOLE, MA   02543

RESIDENT REPRESENTATIVE
OFFICE OF NAVAL RESEARCH
UNIVERSITY OF WASHINGTON
3710 BROOKLYN AVE N E, UNIT 2
SEATTLE, WA   98105

DIRECTOR, INST OF POLAR STUDIES
OHIO STATE UNIVERSITY
125 SOUTH OVAL DRIVE
COLUMBUS, OH   43210

MR PAUL P LAUVER, PUBLICATIONS
ARCTIC INSTITUTE OF NORTH AMERICA
3426 NO WASHINGTON BLVD
ARLINGTON, VA   22201

COMMANDER
NAVAL UNDERSEA CENTER
ATTN TECHNICAL LIBRARY, CODE 1311
SAN DIEGO, CA   92132

DR KENNETH L HUNKINS
LAMONT-DOHERTY GEOLOGICAL OBSERVATORY
TORREY CLIFFE
PALISADES, N Y   10964

SUPERINTENDENT
NAVAL POSTGRADUATE SCHOOL
LIBRARY CODE 2124
MONTEREY, CA   93940

DR E R POUNDER
RUTHERFORD PHYSICS BUILDING
MCGILL UNIVERSITY
3600 UNIVERSITY STREET
MONTREAL, PQ CANADA   H3A 2T8

MR BEAUMONT BUCK
POLAR RESEARCH LABORATORY INC
123 SANTA BARBARA STREET
SANTA BARBARA, CA   93101

DR WARREN DENNER
NAVAL ARCTIC RESEARCH LABORATORY
BARROW, AK   99723

DR V P HESSLER
4230 EUTAW STREET
BOULDER, CO   80302

CHIEF OF NAVAL RESEARCH CODE 480D
OFFICE OF NAVAL RESEARCH
ARLINGTON, VA   22217

DR. KOU KUSUNOKI
NATIONAL INSTITUTE OF POLAR RESEARCH
KAGA 1-9-10, ITABASHI-KU
TOKYO, JAPAN

CAPTAIN D C NUTT, USN (RET)
DEPARTMENT OF GEOGRAPHY
DARTMOUTH COLLEGE
HANOVER, NH   03755

DR T E ARMSTRONG
SCOTT POLAR RESEARCH INSTITUTE
CAMBRIDGE, CB2 1ER
ENGLAND

MISS MOIRA DUNBAR
DEFENCE RESEARCH ESTABLISHMENT
OTTAWA, NATL DEFENCE HEADQUARTERS
OTTAWA, ONTARIO K1A 0Z4, CANADA

DR A R MILNE
DEFENCE RESEARCH ESTABL PACIFIC
FLEET MAIL OFFICE
VICTORIA, BRITISH COLUMBIA, CANADA

DR SVENN ORVIG
MCGILL UNIVERSITY
DEPT OF METEOROLOGY
P O BOX 6070
MONTREAL 101, QUEBEC, CANADA

DEPARTMENTAL LIBRARY-SERIALS
DEPARTMENT OF THE ENVIRONMENT
OTTAWA, CANADA K1A 0H3

DR K M RAE
VICE PRESIDENT FOR RESEARCH
UNIVERSITY OF ALASKA
FAIRBANKS, AK   99701

DR ROBERT L RAUSCH
DEPARTMENT OF MICROBIOLOGY
WESTERN COLLEGE OF VET MEDICINE
UNIVERSITY OF SASKATCHEWAN
SASKATOON, SASKATCHEWAN, CANADA
S7N 0W0

DR HECTOR R FERNANDEZ
DEPARTMENT OF BIOLOGY
UNIV OF SOUTHERN CALIFORNIA
LOS ANGELES, CA   90007

DR GEORGE A LLANO
ACTING CHIEF SCIENTIST
OFFICE OF POLAR PROGRAMS
NATIONAL SCIENCE FOUNDATION
WASHINGTON, D C   20550

MR WALTER I WITTMAN
NAVAL OCEANOGRAPHIC OFFICE
CODE 7600
WASHINGTON, D C   20390

MR LOUIS DEGOES
EXECUTIVE SECRETARY
POLAR RESEARCH BOARD
NATIONAL ACADEMY OF SCIENCES
2101 CONSTITUTION AVENUE, N W
WASHINGTON, D C   20418

DR HARLEY J WALKER
DEPARTMENT OF GEOGRAPHY
LOUISIANA STATE UNIVERSITY
BATON ROUGE, LA   70803

DR JOHN C F TEDROW
DEPARTMENT OF SOILS, LIPMAN HALL
RUTGERS UNIVERSITY
NEW BRUNSWICK, NJ   08903

MR M M KLEINERMAN
PROJECT MANAGER FOR ARCTIC ASW
U S NAVAL ORDNANCE LABORATORY
WHITE OAK, MD   20910

MR M R HERRMAN
NAVAL FACILITIES ENGINEERING COMMAND
CODE 032A, YARDS & DOCKS ANNEX ROOM 2B1
WASHINGTON, D C   20390

NORSK POLARINSTITUTT
ROLFSTANGVN 12, POSTBOKS 158
1330 OSLO LUFTHAVN, NORWAY

PROF WILLIAM MCINTIRE
COASTAL STUDIES INSTITUTE
LOUISIANA STATE UNIVERSITY
BATON ROUGE, LA   70803

DR W M SACKINGER
DEPT OF ELECTRICAL ENG
UNIVERSITY OF ALASKA
FAIRBANKS, AK   99701

MANAGER, INUVIK RESEARCH LAB
BOX 1430
INUVIK, N W TERRITORIES XOE OTO
CANADA

DR WESTON BLAKE, JR
GEOLOGICAL SURVEY OF CANADA
DEPT OF ENERGY, MINES & RESOURCES
601 BOOTH STREET
OTTAWA, ONTARIO K1A OE8, CANADA

CHIEF OF NAVAL RESEARCH
OFFICE OF NAVAL RESEARCH CODE 412
ARLINGTON, VA   22217

CHIEF OF NAVAL RESEARCH
OFFICE OF NAVAL RESEARCH CODE 414
ARLINGTON, VA   22217

NATIONAL INST OF OCEANOGRAPHY
WORMLEY, GODALMING
SURREY, ENGLAND

MRS CARMEN R JOHNSON
PHYSICAL OCEANOGRAPHER
SEARCH & ACQUISITION BRANCH
NATL OCEANOGRAPHIC DATA CENTER
WASHINGTON, D C   20390

DR ING O MAGGIOLO
FACULTAD DE INGENIERIA
HERRERA Y REISSIG 585
MONTEVIDIO, URUGUAY

MRS GAIL HORWOOD
METEOROLOGY LIBRARY
MCGILL UNIVERSITY
MONTREAL, QUEBEC, CANADA

DR CHARLES E BEHLKE, DIRECTOR
INST OF ARCTIC ENVM ENGINEERING
UNIVERSITY OF ALASKA
COLLEGE, AK   99701

WORLD DATA CENTER: A FOR GLAC
INST OF ARCTIC & ALPINE RESEARCH
UNIVERSITY OF COLORADO
BOULDER, CO   80309

METEOROLOGICAL OFFICE LIBRARY
LONDON ROAD
BRACKNELL, BERKSHIRE, ENGLAND

PROF DR ALEXSANDER KOSIBA
KATEFRA I OBSERWATORIUM
METEOROLOGI I KLIMATOLOGII
UNIWERSYTETN WROCLAWSKIEGO
WROCLAW 9, U..CMENTARNA 8, POLAND

CENTRE NATIONAL DE LA RECHERCHE SCIENTIFIQUE
LABORATOIRE DE GLACIOLOGIE
UNIVERSITE DE GRENOBLE 1
SERVICE DE GEOPHYSIQUE
2, RUE TRES-CLOITRES
38-GRENOBLE, FRANCE

CENTRE D'ETUDES ARCTIQUES
ECOLE PRATIQUE DES HAUTES ETUDES
VI SECTION (SORBONNE)
6, RUE DE TOURNON
PARIS-6, FRANCE

STOCKHOLMS UNIVERSITET
NATURGEOGRAFISKA INSTITUTIONEN
BOX 6801
113 86 STOCKHOLM, SWEDEN

DR E L LEWIS
FROZEN SEA RESEARCH GROUP
INSTITUTE OF OCEAN SCIENCES
9860 W SAANICH ROAD
SIDNEY B.C. CANADA   V8L-3S2

PROF F KENNETH HARE
DIRECTOR-GENL OF RESEARCH COORDINATION
ENVIRONMENT-CANADA (P P AND R)
OTTAWA K1A OH3, ONTARIO, CANADA

POLAR INFORMATION SERVICE
OFFICE OF POLAR PROGRAMS
NATIONAL SCIENCE FOUNDATION
WASHINGTON, D C   20550

DR DONALD W HOOD
INSTITUTE FOR MARINE SCIENCE
UNIVERSITY OF ALASKA
FAIRBANKS, AK   99701

DR LAWRENCE COACHMAN
DEPARTMENT OF OCEANOGRAPHY
UNIVERSITY OF WASHINGTON
SEATTLE, WA   98195

MARINE SCIENCES CENTRE LIBRARY
MCGILL UNIVERSITY
P O BOX 6070
MONTREAL 101, QUEBEC, CANADA

DR DAVID CLARK
DEPARTMENT OF GEOLOGY
UNIVERSITY OF WISCONSIN
MADISON, WI   53706

DR ARTHUR LACHENBRUCH
BRANCH OF GEOPHYSICS
U S GEOLOGICAL SURVEY
345 MIDDLEFIELD ROAD
MENLO PARK, CA   94025

DEFENCE RESEARCH BOARD
DEPT OF NATIONAL DEFENCE
190 O'CONNOR STREET
OTTAWA, ONTARIO K1A OZ3, CANADA

DR T SAUNDERS ENGLISH
DEPT OF OCEANOGRAPHY
UNIVERSITY OF WASHINGTON
SEATTLE, WA   98195

DR KEITH MATHER
GEOPHYSICAL INSTITUTE
UNIVERSITY OF ALASKA
COLLEGE, AK   99701

CONTRACT ADMINISTRATOR
OFFICE OF NAVAL RESEARCH BR OFFICE
1030 EAST GREEN STREET
PASADENA, CA   91106

THE LIBRARIAN
SCOTT POLAR RESEARCH INST
CAMBRIDGE CB2 1ER

LIBRARIAN (CODE 1640)
U S NAVAL OCEANOGRAPHIC OFFICE
SUITLAND, MD   20390

RESEARCH LIBRARY
NAVAL ELECTRONICS LAB CENTER
SAN DIEGO, CA   92152

LIBRARIAN, TECH LIBRARY DIV
NAVAL CIVIL ENG LABORATORY
PORT HUENEME, CA   93041

DR ALBERT H JACKMAN
CHAIRMAN DEPT OF GEOGRAPHY
WESTERN MICHIGAN UNIVERSITY
KALAMAZOO, MI   49001

MR ROBERT D KETCHUM JR
BLDG 70, CODE 8050
NAVAL RESEARCH LAB
WASHINGTON, D C   20390

PROF RICHARD S TANKIN
DEPT OF MECHANICAL ENG
NORTHWESTERN UNIVERSITY
EVANSTON, IL   60201

DR GUNTER WELLER
GEOPHYSICAL INSTITUTE
UNIVERSITY OF ALASKA
COLLEGE, AK   99701

DR KNUT AAGARD
DEPT OF OCEANOGRAPHY
UNIVERSITY OF WASHINGTON
SEATTLE, WA   98195

REPORT DOCUMENTATION PAGE	READ INSTRUCTIONS BEFORE COMPLETING FORM	
1. REPORT NUMBER SCIENTIFIC REPORT NO. 15	2. GOVT ACCESSION NO.	3. RECIPIENT'S CATALOG NUMBER
4. TITLE (and Subtitle) BRINE DRAINAGE AND CONVECTION IN YOUNG SEA ICE		5. TYPE OF REPORT & PERIOD COVERED SCIENTIFIC REPORT NO. 15
		6. PERFORMING ORG. REPORT NUMBER
7. AUTHOR(s) TERREN MARK NIEDRAUER		8. CONTRACT OR GRANT NUMBER(s) N00014-76-C-0234
9. PERFORMING ORGANIZATION NAME AND ADDRESS ARCTIC SEA AIR INTERACTION UNIVERSITY OF WASHINGTON, SEATTLE, WA 98195 DEPARTMENT OF ATMOSPHERIC SCIENCES, AK-40		10. PROGRAM ELEMENT, PROJECT, TASK AREA & WORK UNIT NUMBERS NR 307-252
11. CONTROLLING OFFICE NAME AND ADDRESS OFFICE OF NAVAL RESEARCH CODE 461, ARCTIC PROGRAM ARLINGTON, VIRGINIA 22217		12. REPORT DATE 1977 July. 13. NUMBER OF PAGES 72
14. MONITORING AGENCY NAME & ADDRESS(if different from Controlling Office)		15. SECURITY CLASS. (of this report) UNCLASSIFIED
		15a. DECLASSIFICATION/DOWNGRADING SCHEDULE

16. DISTRIBUTION STATEMENT (of this Report)

THE DISTRIBUTION OF THIS REPORT IS UNLIMITED

17. DISTRIBUTION STATEMENT (of the abstract entered in Block 20, if different from Report)

18. SUPPLEMENTARY NOTES

19. KEY WORDS (Continue on reverse side if necessary and identify by block number)

SEA ICE
    Desalination   Brine convection
    Thermodynamics   Brine pockets
    Brine channels

20. ABSTRACT (Continue on reverse side if necessary and identify by block number)

In a series of experiments using a 1.6 mm thick freezing tank, thin sections of salt water ice were grown which exhibit the same drainage features as natural sea ice. The tank design permitted photographs to be taken, while thermocouples mounted in the tank walls recorded the temperature profiles within the ice. Convection was observed in both the skeleton layer and in the brine channels by the flow of dyed brine. Flow in the skeleton layer was cusp-like in appearance, consisting of narrow downflow regions separated

DD FORM
1 JAN 73 1473   EDITION OF 1 NOV 65 IS OBSOLETE
S/N 0102-014-6601 |

20. by broad upflow regions. Several brine channels were usually present in the ice and convective overturning occurred in these channels. The convection caused temperature fluctuations of 0.05°C, which calculations show increase the vertical heat flux by 2%. The brine drainage channels, which were usually sloped 30° to 60° to the horizontal, always had isotherms tilted from 0° to 13° in the same direction. The brine channels move both horizontally and vertically through the ice by melting their lower walls and freezing on the upper walls. An analysis based on the heat flux due to brine channel convection shows that convection can drive these wall movements. Our observations suggest that most of the brine movement in the channels is caused by recirculation of water from below the ice. We also observed the formation of brine pockets from brine tubes.